Atmos. Chem. Phys., 11, 8103–8131, 2011
www.atmos-chem-phys.net/11/8103/2011/
doi:10.5194/acp-11-8103-2011
© Author(s) 2011. CC Attribution 3.0 License.

Atmospheric Chemistry and Physics

Representation of tropical deep convection in atmospheric models – Part 2: Tracer transport

C. R. Hoyle[1,2], V. Marécal[5], M. R. Russo[7], G. Allen[14], J. Arteta[5], C. Chemel[4], M. P. Chipperfield[3], F. D'Amato[11], O. Dessens[10], W. Feng[3], J. F. Hamilton[12], N. R. P. Harris[9], J. S. Hosking[10,], A. C. Lewis[12], O. Morgenstern[7,*], T. Peter[1], J. A. Pyle[7], T. Reddmann[8], N. A. D. Richards[3], P. J. Telford[9], W. Tian[3], S. Viciani[11], A. Volz-Thomas[13], O. Wild[6], X. Yang[10], and G. Zeng[7,*]**

[1]Institute for Atmospheric and Climate Science, ETH Zurich, Zurich, Switzerland
[2]Department of Geosciences, University of Oslo, Norway
[3]Institute for Climate and Atmospheric Science, School of Earth and Environment, University of Leeds, UK
[4]NCAS-Weather, Centre for Atmospheric & Instrumentation Research, University of Herfordshire, UK
[5]Centre National de Recherches Météorologiques/Groupe d'étude de l'Atmosphére Météorologique, Météo-France and CNRS, Toulouse, France
[6]Lancaster Environment Centre, Lancaster University, UK
[7]NCAS climate, Centre for Atmospheric Science, Department of Chemistry, University of Cambridge, UK
[8]Institute for Meteorology and Climate Research, Karlsruhe Institute of Technology, Karlsruhe, Germany
[9]European Ozone Research Coordinating Unit, University of Cambridge Department of Chemistry, Lensfield Road, Cambridge CB2 1EW, UK
[10]Centre for Atmospheric Science, University of Cambridge, Cambridge, UK
[11]CNR-INO (Istituto Nazionale di Ottica) Largo E. Fermi, 6 50125 Firenze, Italy
[12]University of York, Heslington, York, YO105DD, UK
[13]Institute for Energy and Climate Research, Forschungszentrum Jülich, Germany
[14]Centre for Atmospheric Science, University of Manchester, Manchester, UK
[*]now at: National Institute of Water and Atmospheric Research, Lauder, New Zealand
[**]now at: British Antarctic Survey, Cambridge, UK

Received: 5 July 2010 – Published in Atmos. Chem. Phys. Discuss.: 27 August 2010
Revised: 19 June 2011 – Accepted: 12 July 2011 – Published: 9 August 2011

Abstract. The tropical transport processes of 14 different models or model versions were compared, within the framework of the SCOUT-O3 (Stratospheric-Climate Links with Emphasis on the Upper Troposphere and Lower Stratosphere) project. The tested models range from the regional to the global scale, and include numerical weather prediction (NWP), chemical transport, and chemistry-climate models. Idealised tracers were used in order to prevent the model's chemistry schemes from influencing the results substantially, so that the effects of modelled transport could be isolated. We find large differences in the vertical transport of very short-lived tracers (with a lifetime of 6 h) within the tropical troposphere. Peak convective outflow altitudes range from around 300 hPa to almost 100 hPa among the different models, and the upper tropospheric tracer mixing ratios differ by up to an order of magnitude. The timing of convective events is found to be different between the models, even among those which source their forcing data from the same NWP model (ECMWF). The differences are less pronounced for longer lived tracers, however they could have implications for modelling the halogen burden of the lowermost stratosphere through transport of species such as bromoform, or short-lived hydrocarbons into the lowermost stratosphere. The modelled tracer profiles are strongly influenced by the convective transport parameterisations, and different boundary layer mixing parameterisations also have a large impact on the modelled tracer profiles. Preferential locations for rapid transport from the surface into the upper troposphere are similar in all models, and are mostly concentrated over the western Pacific, the Maritime Continent and the Indian

Correspondence to: C. R. Hoyle
(christopher.hoyle@env.ethz.ch)

Published by Copernicus Publications on behalf of the European Geosciences Union.

Ocean. In contrast, models do not indicate that upward transport is highest over western Africa.

1 Introduction

The timescales for atmospheric transport and photochemical production/loss are critical, interlinked factors in determining the distribution of trace species in the atmosphere. Short-lived chemical species emitted at the Earth's surface are removed in the lower troposphere unless they encounter meteorological conditions that result in fast upward transport to the upper troposphere or lower stratosphere (UT/LS). In the tropics, rapid vertical transport can be achieved within individual thunderstorms and larger areas of convection. However, the amount of short-lived species which reach the UT/LS is not known with great confidence from either observational or modelling studies (Law and Sturges, 2007). Recently the issue has received even greater attention since the contribution of very short-lived bromocarbons to the stratospheric bromine budget, and therefore to stratospheric ozone concentrations, has been recognised as a potentially important term (e.g. Sturges et al., 2000; Salawitch et al., 2005; Sinnhuber and Folkins, 2006; Feng et al., 2007; Laube et al., 2008; Hossaini et al., 2010; Liang et al., 2010). In addition, fast transport is important in determining the atmospheric distributions of other natural, short-lived species (e.g. hydrocarbons and their breakdown products) as well as anthropogenic pollutants such as CO, C_2H_2 (Park et al., 2008) and, by implication, NO_x. The lifetime of such short-lived species, once in the UT/LS, is largely determined by the altitude at which they are detrained from the convective column.

Short-lived halocarbons such as bromoform and dibromomethane, are likely to contribute to part, if not all, of the reported "missing" bromine in the stratospheric bromine budget; in order to understand the role of these gases in stratospheric ozone depletion it is therefore important to quantify their vertical transport from the surface to a region of upward motion (Sinnhuber and Folkins, 2006).

In the tropics there is a gradual transition from tropospheric to stratospheric chemical and dynamical regimes, known as the tropical tropopause layer (TTL) (e.g. Fueglistaler et al., 2009, and references therein). Net upward motion occurs above the level of zero radiative heating, which is where radiative heating becomes positive and air rises. The height of the zero radiative heating level depends on the local temperature profile, the water vapour mixing ratio and whether or not clouds are present (e.g. Hartmann and Larson, 2002; Corti et al., 2005). A typical value is 15 km (ca. 120 hPa) (Sherwood and Dessler, 2000), which is above the level of main convective outflow (about 12–13 km, or 195–165 hPa) (Folkins et al., 1999, 2000). As a result, only a small fraction of the air lofted up in convective towers reaches this higher level, and therefore the relative fraction of surface air which is convectively lofted to the zero radiative heating level, and eventually reaches the stratosphere, is determined by the tail of the distribution of convective outflow heights. This is not well known from either observational or modelling studies, and there has recently been considerable debate on this matter (e.g. Kupper et al., 2004; Ricaud et al., 2007; Fueglistaler et al., 2009).

Data from model runs using different moist convection and boundary layer schemes was compared by Mahowald et al. (1995), which suggested that the mid-and-upper tropospheric profiles of atmospheric species may not be particularly sensitive to the boundary layer scheme used, while using different convection parameterisation schemes had a larger impact. Lawrence and Rasch (2005) compared the plume ensemble formulation and a bulk formulation of convective transport in the MATCH chemical transport model, and found that the bulk formulation, which has a greater rate of mid-tropospheric entrainment, results in significantly less transport into the upper troposphere compared to the plume ensemble approach.

A number of studies have tried to quantify the effect of different model formulations and convection parameterisations on the height of the main convective outflow and the efficiency of convective transport. Folkins et al. (2006) compared two convective parameterisations in a one-dimensional framework as well as two further parameterisations in the GEOS-3 and GEOS-4 global models: using climatologies of CO, H_2O, HNO_3 and O_3 for comparison with model data, they found that models with a clearly defined convective outflow layer in the region of 10–13 km (or ca. 265–165 hPa) matched the measurements best. Arteta et al. (2009a) used an online regional model, CATT-BRAMS, to investigate the sensitivity of tropical tracer transport to the convective parameterisation, and Arteta et al. (2009b) evaluated the effect of resolution on the simulated tracer distributions, showing that the higher resolution versions of their model exhibited more efficient convective transport, reaching higher altitudes. Various studies (Deng et al., 2004; Wild and Prather, 2006; Rind et al., 2007) have shown that increased horizontal and vertical resolution improves the skill of the model in predicting tracer transport by convection. Five different convective parameterisations were investigated in the chemistry-climate model ECHAM5/MESSy, by Tost et al. (2010), who found mean differences between the convection schemes of less than 25 % for long-lived tracers, and up to 100 % for short-lived tracers. They attribute these differences not only to the strength and frequency of convective events, but also to processes such as wet scavenging, and chemistry, which are also affected by the transport of species to different regions. The chemistry-climate model STOCHEM-HadAM3 was used by Doherty et al. (2005) to investigate the influence of convection on upper tropospheric O_3. They find that the effect of convective overturning decreases the concentration of O_3 in the upper troposphere, despite a positive contribution from changes in O_3 chemistry associated with the

convective transport. It is further pointed out by Doherty et al. (2005) that their results contrast with the increase in global O_3 simulated by Lawrence et al. (2003) with a similar model. They suggest that this could be due to model differences in convective mixing.

Upper tropospheric O_3 and CO data from four chemical transport models was used by Barret et al. (2010) which found general agreement between models, and showed that elevated CO and O_3 observations were due to convective uplift of biomass burning emissions. Barth et al. (2007) compared the transport of several chemical species in eight models. They found longer lived species such as O_3 and CO to compare well between models, although substantial differences were found in the predicted mixing ratios of soluble species in the cloud anvil.

In this set of two papers we attempt to evaluate and compare the transport of short-lived tracers in many of the global and mesoscale models used within the SCOUT-O3 project. These include chemical transport models, coupled chemistry-climate models, general circulation models and a mesoscale model. Various differences exist between the models in this study, such as resolution, boundary layer schemes and convective transport parameterisations, as well as the methods used to calculate the vertical winds, even when the same meteorological data is used (for the offline models). All these factors contribute to differences in the modelled tracer profiles. Some of the model configurations used in this paper only differ in one aspect (see Sect. 2), allowing us to attribute differences in transport between some of the models.

In the first paper Russo et al. (2011), (hereafter R_2011), we evaluated the models' convection by comparison of modelled meteorological parameters to satellite observations. The main findings of this analysis were as follows: the frequency and distribution of cloud top heights reaching above 15 km varied largely between different models; the models represented reasonably well the average values and observed seasonal cycle of precipitation rates (used as a proxy for convection) for continental regions, however larger discrepancies with observations were found for the Maritime Continent, an important region for convective transport.

In this second paper we compare the modelled vertical transport of tracers. This task is hampered by the lack of an observational quantity which can be considered as "truth": uncertainties in emissions and in chemical degradation schemes limit the degree to which any discrepancies can be ascribed to the transport schemes. Therefore, the core of our comparison is based on idealised tracers which are prescribed in the same way for all models. These can reveal model differences but do not in themselves indicate which model's transport scheme is best. To shed light on the latter issue, a semi-realistic tracer (idealised CO) is used and compared to measurements. Since the primary source of CO in the troposphere is at the surface, it is a good tracer to study upward vertical transport.

In Sect. 2 of this paper, the models and their setups are described. The rationale for the choice of the idealised tracers and their characteristics are explained in Sect. 3, and in Sect. 4, we describe the measurements datasets used for comparison with model data. Results are described in Sect. 5, focusing on specifically on tracer profiles in the Tropics (Sect. 5.1), the strength and spatial distribution of tropical convection (Sect. 5.2), and a comparison of the idealised CO with measurements (Sect. 5.3). The main conclusions are drawn in Sect. 6, as well as discussing the lessons learnt from comparison of the models' representation of tracer transport in strongly convective regions.

2 Models

A total of 14 models, or model versions, participated in this inter-comparison: 7 global off-line chemical transport model (CTM) simulations, 4 coupled chemistry-climate models (CCMs) and 3 numerical weather prediction (NWP) models. An initial series of modelling experiments were run, Round 1 (R1), and based on the results of these, the tracers were refined and a second set of experiments was carried out Round 2 (R2). A summary of the configuration of these runs is provided in Table 1. The CTM, and nudged CCM model simulations were run for the year 2005, the un-nudged CCMs used boundary conditions representative of this time period. The NWP model WRF was run for February, August and November 2005, and CATT-BRAMS was run for the Maritime Continent area for November 2005. The models are described below.

2.1 TOMCAT CTM

TOMCAT is a 3-dimensional CTM with a variable horizontal and vertical resolution (Chipperfield, 2006). The model is forced using 6-hourly ECMWF analyses for vorticity, divergence, humidity and temperature. The vorticity and divergence fields provide the large-scale horizontal winds and vertical winds are diagnosed from the analysed divergence. Sub-grid scale transport is parameterised in the model using information from the large-scale analyses.

The convection scheme implemented in TOMCAT is similar to the scheme described by Tiedtke (1989), which uses a bulk model to represent an ensemble of shallow, midlevel and deep convective clouds. In TOMCAT, mid-level convection and convective down-drafts are not included and there is no organised entrainment of environmental air above cloud base (Stockwell and Chipperfield, 1999). The scheme does include cumulus up-drafts in the vertical column entrainment of environmental air into the cloud and detrainment of cloud air to the environment. The magnitudes of these are related to horizontal convergence of moisture below cloud and the difference between cloud and environmental specific humidity at cloud base. Mass balance within the vertical column is

Table 1. The models which participated in the inter-comparison. The models were run at the following institutions: [1,5,8] University of Leeds, [2] Karlsruhe Institute of Technology, [3,4,9,10,11,12] University of Cambridge, [6] University of Oslo, [7] Lancaster University, [13] Météo-France and CNRS and University of Orléans, [14] University of Herfordshire.

Model	Type	Resolution	Transport	BL mix.	Circulation	Reference
			Round 1			
[1]TOMCAT_Louis	CTM	2.8°×2.8°L31	Prather (1986)	Louis (1979)	ECMWF operational	Tiedtke (1989)
[2]KASIMA	CTM	5.6°×5.6°, 750 m	Zalesak (1979)	no BL	ECMWF operational	none
[3]UMCAM	CCM	2.5°×3.8°L19	Leonard et al. (1995)	see text	N/A	Gregory and Rowntree (1990)
[4]UMUKCA-UCAM (R1)	CCM	2.5°×3.8°L38	semi-Lagrangian	Lock et al. (2000)	N/A	Gregory and Rowntree (1990)
[5]UMSLIMCAT	CCM	2.5°×3.8°L64	Gregory and West (2002)	no mixing	N/A	Gregory and Rowntree (1990)
			Round 2			
[6]Oslo CTM2	CTM	2.8°×2.8°L40	Prather (1986)	Holtslag et al. (1990)	ECMWF IFS cycle 29	see text
[7]FRSGC/UCI	CTM	2.8°×2.8°L37	Prather (1986)	Holtslag et al. (1990)	ECMWF IFS cycle 29	see text
[8]TOMCAT (R2)	CTM	2.8°×2.8°L31	Prather (1986)	Holtslag and Boville (1993)	ECMWF operational	Tiedtke (1989)
[9]pTOMCAT	CTM	2.8°×2.8°L31	Prather (1986)	Holtslag and Boville (1993)	ECMWF operational	Tiedtke (1989)
[10]pTOMCAT-tropical	CTM	2.8°×2.8°L31	Prather (1986)	Holtslag and Boville (1993)	ECMWF operational	Barret et al. (2010)
[11]UMUKCA-UCAM_nud	nudged CCM	2.5°×3.8°L38	Priestley (1993)	Lock et al. (2000)	Nudged with ECMWF operational	Gregory and Rowntree (1990)
[12]UM-UCAM_highres	global NWP	0.6°×0.8°L38	Priestley (1993)	Lock et al. (2000)	Initialised from UKMO	Gregory and Rowntree (1990)
[13]CATT-BRAMS	Regional NWP	60km x 60km L39	Tremback et al. (1987)	Mellor and Yamada (1982)	Initialised from ECMWF	Grell and Dévényi (2002)
[14]WRF	global NWP	1.9°×1.3°L38	Skamarock et al. (2008)	Sukoriansky et al. (2005)	Initialised from ECMWF	Grell and Dévényi (2002)

maintained by including sub-grid subsidence of environmental air (induced by convection) within the same time step.

Two TOMCAT runs were performed. For the simulation TOMCAT_Louis the model was run at $2.8° \times 2.8°$ with 31 hybrid σ-p levels from the surface to 10 hPa. This run used the boundary layer (BL) mixing scheme of Louis (1979), which is a local scheme, where only the local gradients in wind shear and lapse rate are calculated, and it is assumed that vertical diffusion can be treated similarly to molecular diffusion (Stockwell and Chipperfield, 1999). The limitations of this kind of scheme are that it does not account for entrainment at the top of the BL, and that it cannot account for eddy transport of tracers throughout the BL. This leads to less mixing within the BL, and between the BL and the free troposphere, compared to a non-local scheme such as that of Holtslag and Boville (1993). Furthermore, the Louis (1979) BL mixing scheme produces low BL heights (Wang et al., 1999).

TOMCAT_R2 is similar to TOMCAT_Louis except that the non-local boundary layer mixing scheme of Holtslag and Boville (1993) was used, leading to more mixing within the BL, and between the BL and the free troposphere. Instead of using an eddy-diffusivity determined at each point over the vertical extent of the boundary layer, as in the local scheme, the non-local scheme of Holtslag and Boville (1993) determines an eddy diffusivity profile over the diagnosed boundary layer extent, and has the advantage that it may produce significant vertical transport even where the temperature profile is not absolutely unstable across the whole boundary layer height. The same convective parameterisation was used in both TOMCAT_Louis and TOMCAT_R2. Further investigation of the impact of different treatments of convection with the TOMCAT CTM is given in Feng et al. (2011)

2.2 pTOMCAT CTM

pTOMCAT is a global CTM originally derived from TOMCAT. It still uses the same horizontal and vertical coordinates, the same advection and convection schemes and is forced using the same ECMWF analysis files. pTOMCAT has a horizontal resolution of $2.8° \times 2.8°$ and 31 hybrid σ-p levels from the surface to 10 hPa. This run used the non-local boundary layer mixing scheme of Holtslag and Boville (1993), and is therefore very similar to run TOMCAT_R2. pTOMCAT is described in O'Connor et al. (2005).

In pTOMCAT-tropical, the original implementation of the Tiedtke (1989) – based convective mass flux scheme used in p-TOMCAT has been updated to increase convective transport to the mid and upper troposphere (Barret et al., 2010). The entrainment and detrainment rates are set to be half the value suggested by Tiedtke (1989). This means there will be less stable ambient air entrained into the cloud and thus positive buoyancy in the cloud is retained to higher altitudes. This change offsets the problem in off-line models of diagnosing convection with analyses that have already been convectively adjusted. Other changes include using ISCCP satellite cloud data Rossow et al. (1996) to specify the fraction of saturated water vapour in each surface model grid box and putting detrainment at the cloud top layer rather than in each layer between cloud top and bottom to allow a maximum lift for tracers from the boundary layer. The deep convective precipitation is set to be from each layer's newly formed condensed liquid water. This updated scheme is also included in the study of Feng et al. (2011).

2.3 KASIMA CTM

KASIMA is a global CTM, with a lower boundary at a pressure altitude of 4 km. The transport is calculated on a spherical grid with a T21 resolution (approximately $5.6° \times 5.6°$). Advection is calculated using the two-step flux-corrected scheme described by Zalesak (1979). Meteorological data from ECMWF operational analyses is used to drive the model, and the vertical wind is derived from the divergence of the horizontal winds. There is no convective transport, and no boundary layer mixing scheme. For the lower boundary, tracer concentrations were set according to the initial distributions used in the experiments, in a virtual layer below the model domain. When upward vertical winds are present, the tracer is transported from this layer into the model domain. A full model description can be found in Kouker et al. (1999).

2.4 UMCAM CCM

UMCAM is an Eulerian CCM based on the Met Office Unified Model (UM) version 4.5. The horizontal resolution is 2.5° latitude × 3.75° longitude, with 19 vertical layers between the surface and 4.6 hPa. Convection is parameterised using the penetrative mass flux scheme of Gregory and Rowntree (1990), which uses a bulk approach to represent an enseble of shallow, midlevel and deep convective clouds. The boundary layer is mixed using a MOSES-1 Non-local K scheme with entrainment (UKMO surface exchange scheme version 1). Sea surface temperatures and sea ice distribution are prescribed from the BADC dataset for 2005. The model is described in Zeng and Pyle (2003).

2.5 UKCA CCM

UKCA is an Eulerian CCM based on the "new dynamics" version of the Met Office UM (Davies et al., 2005). This model is non-hydrostatic and vertical velocity is calculated as a diagnostic variable on hybrid σ-height coordinates. Not using the hydrostatic approximation allows runs at very high resolution. To increase stability the model uses a two time-level, semi-Lagrangian advection (Priestley, 1993) and semi-implicit time stepping. The model is described in detail in Morgenstern et al. (2009).

As in UMCAM CCM, the convective parameterisation scheme is based on the bulk convection model of Gregory and Rowntree (1990). Both shallow and deep convection are included. Cloud base closure for shallow convection is based on Grant (2001), where the cloud-base mass flux is based on the turbulence kinetic energy budget in the mixed layer below the cloud base. Parameterised entrainment and detrainment rates for shallow convection are obtained from Grant and Brown (1999), assuming that the entrainment and detrainment rates are related to the rate at which turbulence kinetic energy is created in the cloud ensemble. For deep convection, the thermodynamic closure is based on the reduction of convective available potential energy (CAPE) to zero (CAPE closure approach) as in Fritsch and Chappell (1980). The boundary layer parameterisation is based on the non-local boundary layer scheme of Lock et al. (2000). It also includes an explicit parameterisation of entrainment at the boundary-layer top.

Three UKCA runs were performed. Run UMUKCA-UCAM (R1) is a free running version of the UKCA at the usual climate horizontal resolution of N48 (ca. $2.5° \times 3.8°$) and 38 levels from 0 to 39 km.

The nudged model (UMUKCA-UCAM_nud) was run at N48 resolution with 38 levels from 0 to 39 km. The nudged model uses ECMWF operational analyses available every 6 h. This data is interpolated onto the model time-steps and levels. The model temperature and horizontal winds are constrained to this data using the technique of Newtonian relaxation.This version of the model is described in Telford et al. (2008).

UM-UCAM_highres is a higher resolution run of the free-running UKCA model (N216, $0.83° \times 0.56°$) with 38 levels from 0 to 39 km (Petch et al., 2007; Hosking et al., 2010). The model is initialised using UKMO assimilated initial conditions and is constrained by sea surface temperatures and sea ice derived from the GISST 2.0 climatology (Parker et al., 1995).

2.6 UMSLIMCAT CCM

UMSLIMCAT is a coupled chemistry-climate model based on the extended middle atmosphere version of UM version 4.5 (Tian and Chipperfield, 2005). Like UMCAM, the horizontal resolution is 2.5° latitude × 3.75° longitude but the model has 64 vertical levels between the surface and 0.01 hPa. Advection is calculated with the monotonic Quintic-Mono scheme (Gregory and West, 2002), and convection with the bulk penetrative mass flux scheme (Gregory and Rowntree, 1990). There is no mixing of tracers in the boundary layer.

2.7 Oslo CTM2

The Oslo CTM2 is a global CTM, run on 40 vertical levels between the surface and 2 hPa (hybrid σ-p coordinates) for these experiments. The mass centre of the upper model layer is at 10 hPa. The horizontal resolution used here is T42 (approx $2.8° \times 2.8°$). The model uses winds from the ECMWF Integrated Forecast System (IFS) model, with the vertical wind being calculated from the divergence of the horizontal fields. The meteorological input data were generated by running the IFS model at ECMWF in a series of forecasts, started from the analysed fields every 24 h (at 12:00 UTC). Each forecast was run for 36 h, allowing for 12 h of spin-up. Linking together all the forecasts results in a continuous record of input data. Data are sampled every 3 h. The forecasts were run with the cycle 29 version of the IFS model,

with a spectral resolution of T319L40, which is truncated to T42 for the simulations in this study.

As well as providing large-scale winds, the IFS forecasts provide archived convective mass fluxes. The convective transport of tracers is then parameterised as an "elevator system". Starting from the bottom of a model column, the difference in upward mass flux between the top and bottom of a model grid box determines whether entrainment or detrainment to or from the grid box takes place. If there is no difference between the fluxes through the top and bottom of the box, the up-draft simply passes through without any entrainment or detrainment of tracers. The maximum height of convection is determined by the lowest level where either precipitation flux is zero, or upward mass flux is zero. Full mixing of entrained air into the up-draft core is assumed. Turbulent mixing in the boundary layer is treated according to the non-local scheme of Holtslag and Boville (1993). The Oslo CTM2 is described in Berntsen et al. (2006).

2.8 FRSGC/UCI CTM

FRSGC/UCI is a global CTM with a similar configuration to that of the Oslo CTM2. The model was run at T42 resolution for these studies, with 37 vertical layers from the surface to 2 hPa (hybrid σ-p coordinates). The mass centre of the upper model layer is at 10 hPa. The meteorological forcing data is the same as that used by the Oslo CTM2, except that the lowest 5 layers of the 40-layer output are combined into two layers. Convection is parameterised with an elevator approach based on net convective mass fluxes up through the atmospheric column, with additional treatment of explicitly defined entrainment/detrainment fluxes where these are non-zero. The model is described in Wild et al. (2004).

2.9 CATT-BRAMS regional model

CATT-BRAMS is a regional (limited area) meteorological 3-D model including a tracer and aerosol transport model (Freitas et al., 2009). The advection scheme is a flux-form forward-upstream scheme of second order Tremback et al. (1987). Deep and shallow convection are parameterised following the formulation of Grell and Dévényi (2002), as described in Arteta et al. (2009a). This scheme uses a multi-closure and multi-parameter ensemble approach with typically 144 sub-grid members. An ensemble of entrainment/detrainment profiles and/or down-draft parameters is used to determine the vertical redistribution of tracers. Turbulent mixing in the boundary layer is treated according to the level 2.5 scheme of Mellor and Yamada (1982), which employs a prognostic turbulent kinetic energy. The model uses a zero-gradient configuration at the lateral boundaries for both meteorological and tracer variables, except for the normal wind component for which a radiative condition is used according to Klemp and Wilhelmson (1978). In addition, the model is nudged at the lateral and top boundaries with ECMWF 6-hourly analyses. Nudging is carried out over 4 model grid points from the lateral boundaries, with a relaxation timescale of 6 h. For the top boundary, a 3h relaxation timescale is used above 25 km. The horizontal resolution used is 60 km × 60 km ($\sim$0.5° × 0.5°). The simulation uses 39 vertical levels from surface to 40 km. Initial conditions are from ECMWF analyses. Sea surface temperatures are from satellite-derived weekly analyses.

2.10 WRF NWP

WRF version 3.1.1 is a NWP model, run on 38 layers from the surface to 5 hPa using a terrain-following hydrostatic-pressure vertical coordinate system (Skamarock et al., 2008). The horizontal resolution over the global domain is N96 (1.875°longitude by 1.25° latitude) and the time step is 600 s. The model uses the third order Runge-Kutta time splitting advective transport scheme described by Wicker and Skamarock (2002), which is conservative, but not positive definite, nor monotonic. The initial state at the surface and throughout the model atmosphere is derived from the ECMWF analyses at a spectral resolution of T511 (horizontal resolution of about 0.5°). The WRF model physics does not predict sea ice, SST, vegetation fraction, and albedo. These fields are updated in time every 6 h during the model simulation. The deep layer soil temperature is updated every 6 h as well. Sub-grid scale effects of convective and shallow clouds were parameterised by the Betts-Miller-Janjic (BMJ) cumulus scheme (Janjic, 1994, 2000). The non-resolved convective transport of tracers is parameterised using an elevator approach based on the convective mass flux through the atmospheric column (Grell and Dévényi, 2002, as in CATT BRAMS). The mass flux is calculated using precipitation rates and cloud properties. The entrainment/detrainment profile and downdraft parameters are used to determine the vertical redistribution of tracers. Tracers are not chemically active. The surface and boundary layers are represented using the quasinormal scale elimination (QNSE) parameterisation scheme (Sukoriansky et al., 2005).

3 Tracers

The idealised tracers used in the R1 and R2 modelling experiments are listed in Table 2. The tracers' definition, and their role in the analysis of vertical transport are described below:

– **T20** This tracer had a lifetime of 20 days. The initial concentration was 1 pptv at the surface, and zero elsewhere. Throughout the model run the surface concentration was held constant, in the rest of the atmosphere the only loss process for the tracer was decay according to Eq. (1), where t is the time step and τ is the tracer lifetime. This tracer, having a lifetime similar to that of bromoform $CHBr_3$, can be used to assess the differences

Table 2. The idealised tracers used in the experiments More details are provided in the text.

Name	Initial Condition	Source	Lifetime
T20	0	1 pptv at the surface	20 days
T6h	0	1 ppbm at Z<500 m	6 h
CO	0	mixing ratios prescribed at $Z < 700$ hPa	1–3 months (decay rate is a function of pressure)

in short-lived halogenated species reaching the TTL and lowermost stratosphere between different models.

$$C = C_0 e^{-t/\tau} \quad (1)$$

– **T6h** The lifetime of this tracer was 6 h. It was initialised at the beginning of the model run with a zero mixing ratio everywhere in the atmosphere, except between the surface and 500 m, where the mass mixing ratio was set to 1 ppbm. The 1 ppbm condition was maintained in this lower layer throughout the model run. The only loss process was decay according to Eq. (1). Being extremely short-lived, the T6h tracer could be used to investigate very fast transport mechanisms between the surface and the upper troposphere, such as convection. The T6h tracer was also suitable for comparisons with the limited area models, as the short lifetime reduced the influence of transport from the model outer boundaries. Additionally, T6h required shorter spin-up times for the computationally expensive regional models.

– **CO** The idealised CO tracer was initialised from MOPITT data (Deeter et al., 2007) between the surface and 700 hPa. Everywhere else in the atmosphere the initial mixing ratio was zero. Loss of the tracer occurred only via reaction with a prescribed, constant mean OH field with a concentration of 0.5×10^6 molec cm^{-3}. This value is up to a factor of two lower than recent estimates of the global mean OH concentration (e.g. Wang et al., 2008), however it should be noted again that the objective was to create a highly simplified tracer which would behave with some similarity to CO in the atmosphere. Secondary sources of CO from the oxidation of hydrocarbons are also ignored, and the use of a single value for the OH concentration does not take into account latitudinal or seasonal changes in solar radiation (OH concentrations are much higher during the day than the night, and are higher in the tropics than at mid and polar latitudes). The reaction rate was pressure-dependent, given by $k = 1.5 \times 10^{-13} * (1 + 0.6 P_{\mathrm{atm}})$ (Sander et al., 2003), where P_{atm} is pressure (in atmospheres), and k has units of cm^3 molec^{-1} s^{-1}. The CO tracer allows a qualitative validation of modelled transport via comparisons with measured CO distributions.

Table 3. The tracers included in the different model runs.

Model	T20	T6h	CO
TOMCAT_Louis	yes	no	no
KASIMA	yes	no	no
UMCAM	yes	no	no
UMUKCA-UCAM (R1)	yes	no	no
UMSLIMCAT	yes	no	no
Oslo CTM2	yes	yes	yes
FRSGC/UCI	yes	yes	yes
TOMCAT (R2)	yes	yes	yes
pTOMCAT	yes	yes	yes
pTOMCAT-tropical	yes	yes	yes
UMUKCA-UCAM_nud	yes	yes	yes
UM-UCAM_highres	no	yes	no
CATT-BRAMS	no	yes	no
WRF	no	yes	no

The modelling experiments were carried out in two rounds of intercomparisons. In the first round, the basic T20 tracer was used, and based on the results of these experiments, the T6h and CO tracers were included in the second round. Not all models participated in both rounds of the experiments however. Table 3 lists the tracers run in each model. The first five models in Table 3 only participated in the first round of intercomparison, therefore they only ran the T20 tracer. Furthermore, annual mean data for the tropics could not be contributed by three models, UM-UCAM_highres, WRF and CATT-BRAMS. For UM-UCAM_highres and WRF this was because they were only run for the months we focus on here, i.e. February, August and November, and CATT-BRAMS, being a regional model, could not be run for the whole tropical area. This excludes them from the annual, tropical mean comparison using the T6h tracer, which is presented in Sect. 5.1. Due to the long spin-up times required or the lack of chemical solver, UM-UCAM_highres, CATT-BRAMS and WRF could also not include CO or T20.

4 Observational data

In Sect. 5.3, modelled CO is compared with in situ measurements made during the SCOUT-O3 and ACTIVE campaigns, and satellite based measurements made by the Tropospheric Emission Spectrometer (TES).

During the SCOUT-O3 measurement campaign carried out in the area of Darwin, Australia, in November and December 2005, the concentration of CO was measured with the COLD (Cryogenically Operated Laser Diode) instrument on board the Geophysica research aircraft. The COLD instrument is a mid-infrared tunable diode laser airborne spectrometer for in-situ measurement of trace gases. A liquid nitrogen cooled lead-salt diode laser is used in combination with an astigmatic Herriott multi-pass cell (providing an optical path

of 36 m) to detect the absorption signal of the molecules under analysis. A direct absorption detection technique, which does not need in-flight calibration, is employed in conjunction with fast sweep integration. For CO measurements, an in-flight sensitivity of few ppbv is achieved, with a time resolution of 4s, a precision of 1 % and an accuracy in the range of 6 %–9 %, mainly due to the accuracy of the molecular database (Viciani et al., 2008).

The aerosol and chemical transport in tropical convection (ACTIVE) campaign was carried out from Darwin, Australia from November 2005 until February 2006. The aim of the campaign was to quantify the influence of convection on the composition of the TTL (Vaughan et al., 2008). In addition to other measurement platforms, two aircraft were deployed; the NERC-Dornier-228, and the ARA Grob G520T Egrett. While the Dornier conducted measurements up to an altitude of approximately 4 km, the Egrett was used up to around 15km. Fluorescence-based CO measurements were performed aboard both aircraft, with the instrument on the Dornier having an integration time of 10 s, and a detection limit of around 2 ppbv (Allen et al., 2008). The precision of this instrument was ± 2 ppbv, with an accuracy (using a 200 ppbv CO in air calibration gas) of ± 4 ppbv. The calibration gases used for this instrument are tied to the NOAA CO scale. The instrument on the Egrett collected data at a frequency of 1 Hz, a precision of ± 2 ppbv and an accuracy of ± 3 ppbv (5 % at mixing ratios >60 ppb) (Heyes et al., 2009).

TES is an infrared Fourier transform spectrometer which was launched on-board NASA's Aura satellite in 2004 (Beer et al., 2001). TES is the first satellite instrument to provide vertical information on tropospheric ozone whilst simultaneously measuring CO on a global basis. The data used in this study comes from the TES Global Survey operating mode in which TES makes nadir observations with a 5.3×8.3 km footprint, providing near-global coverage approximately every 16 days. TES ozone and CO profiles are provided on 67 vertical levels from the surface to 0.1 hPa and have been extensively validated against in-situ observations (Luo et al., 2007; Nassar et al., 2008; Osterman et al., 2008; Richards et al., 2008; Lopez et al., 2008). In order to correctly compare TES and model profiles one must account for the limited vertical resolution and the effects of a priori information inherent in the retrieved TES profiles. This is achieved through the application of the TES observation operator to the model profile. The observation operator consists of the averaging kernels and the a priori profile used in the retrieval (Rodgers and Connor, 2003). The application of the TES operator to a comparison profile is described in detail in Worden et al. (2007). For this study the unique TES observation operator for each TES profile was applied to each model profile before averaging the resulting profiles for monthly mean comparisons.

5 Results

In this section, the fields of the modelled tracers are compared between the models as well as with observational data. The models have rather different resolutions, and even when the spacing of the grid points is similar, the actual positions often differ. For the comparisons in Sect. 5.1, the data from each model has therefore been linearly interpolated in the necessary spatial and temporal dimensions. By interpolating to a more finely resolved grid than the best model resolution, the smoothing out of peaks or minima was limited. For global plots, such as in Sect. 5.2, the monthly mean model data were linearly interpolated to the same grid as the Oslo CTM2, in order to compare identical pressure levels. Several of the models did not run all of the experiments, therefore some models are not included in each of the plots shown below.

5.1 Tropical concentration profiles

We start our analysis with the T6h tracer; this tracer's mixing ratio decreases by half in $\sim$4 h and goes to zero after $\sim$24 h. Because of its extremely short lifetime, this tracer can only experience fast transport processes and its vertical profile will be therefore mainly affected by convective transport. To analyse the convective transport in the different models using T6h (and T20 in the next section), we focus on the Tropics (20° N–20° S) as well as three specific geographical regions, namely South America, West Africa and the Maritime Continent (hereafter abbreviated as SA, WA and MC), which have been chosen to provide examples of different types of land and island deep convection. These regions are the same as in R_2011, and are shown in Fig. 1

In R_2011, we performed a detailed comparison of modelled and observed cloud top height distributions to investigate differences in the strength of the convection and the ability of convective parameterisations to reproduce the observed vertical distributions of clouds. Here we investigate how the same convective parameterisations differ in the vertical transport of tracers. In particular, we focus on the height of the mean convective outflow and the tracer's peak concentrations at the outflow relative to the surface concentration. If one compares the same model in different regions, the changes in the height of the tracer's main convective outflow should be determined by changes in the vertical extent of the convection, while the changes in tracer's peak concentration at the outflow should follow changes in the number of convective events reaching that height. However, differences between models are not always directly attributable to such changes. In fact, the way models parameterise venting of the boundary layer, and the values of entrainment-detrainment rates in the convective plume, can have a larger impact on the tracer distribution than the vertical extent or frequency of the convection. For example, some models use convective schemes which release the tracer at the top of the convection

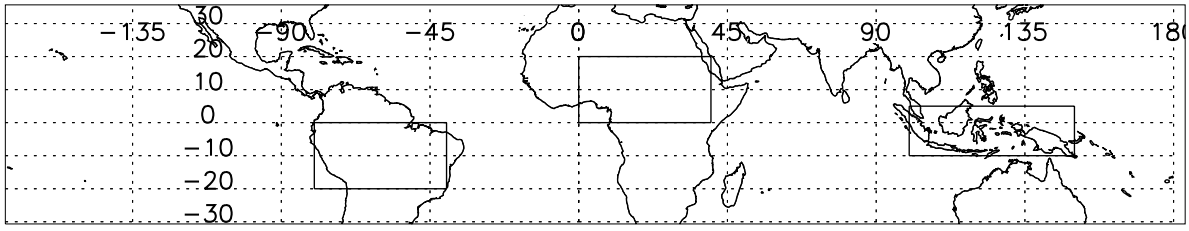

Fig. 1. The rectangles show the regions which were examined in this study, South America, West Africa and the Maritime Continent.

while others distribute the tracer throughout the convective column. Therefore, one should keep in mind that differences between models' vertical profiles of T6h are not always directly attributable to differences in the vertical extent of the convection or the number of convective events. For this reason, the meteorological analysis of convective properties in R_2011 will help to attribute differences in the models' convective transport.

The convective transport in each of the three regions is analysed for one month, during which the region exhibits a strong convective activity (see R_2011 for further discussion on the choice of the regions and the respective months). The monthly mean vertical profiles of T6h are shown in Fig. 2, averaged over SA in February, WA in August and MC in November. Additionally we show for comparison the annual mean tracer profile averaged over the whole tropical region (note that only a subset of the models have archived the necessary information for this plot).

We first analyse the height of the mean convective outflow and how it varies between models and between different geographical locations compared to the tropical mean. For the tropical region, we can distinguish between two sets of models, those with a mean convective outflow at a height of ∼190 hPa (∼12.5 km) and those with a lower convective outflow at ∼300 hPa (∼9 km). These two model categories are also clearly marked for SA, with outflow heights at 190–200 hPa and 300 hPa respectively. Radar reflectivity data was used by Mullendore et al. (2009) to investigate the level of detrainment in a convective storm observed over Brazil during January 1999. For this particular event, the maximum detrainment was found to be at around 11 km, or approximately 220 hPa, which is not greatly different than either of the sets of models.

For the MC region the outflow heights of the first set of models are further split between ∼150 hPa (∼14 km) for CATT-BRAMS and pTOMCAT_tropical, and 190–200 hPa for most other models, while TOMCAT and pTOMCAT outflow heights remain around 300 hPa. For the WA region, differences in the height of the convective outflow are smaller, with values of ∼180–200 hPa for most models and 250 hPa (∼10.5 km) for TOMCAT and pTOMCAT. The lower outflow heights displayed by TOMCAT and pTOMCAT can be explained by the cloud top height analysis in R_2011: with the exception of the WA region, these two models show a consistently smaller percentage of clouds reaching above 10 km compared to observations and other models. This indicates that the vertical extent of tropical convection, and the associated fast vertical transport, might be underestimated in these models.

Most of the models are either forced by or nudged to ECMWF winds (the only exceptions in Fig. 2 being WRF, CATT-BRAMS and UM-UCAM_highres). The span of results between the different models shows that the short-lived tracer transport depends more on the details of the convective parameterisation than on the forcing data, or the model resolution. Indeed, Oslo CTM2 and FRSGC/UCI use virtually identical wind fields, and while they have very similar outflow heights, lower down in the model profiles there are significant differences, for example at 600–700 hPa over the MC and WA, and 300 hPa and below over WA, which appear to be related to the representation of the boundary layer.

Modifying the convective parameterisation scheme in pTOMCAT (pTOMCAT_tropical, shown as the dashed line in Fig. 2) produces cloud top heights which are in better agreement with observations (see also R_2011); the tracer's convective outflow for this modified version is also significantly higher, and very similar to the high resolution CATT-BRAMS model, which uses its own dynamics as opposed to ECMWF forcing. A comparison of convective transport in pTOMCAT_tropical with other models, and with observations, was also presented in Barret et al. (2010), where the modelled deep convective mass flux for August 2006 was found to reach approximately 170 hPa, similar to the maximum outflow height of pTOMCAT_tropical shown here, and within the range of outflow heights produced by other models included in that study (125 hPa–200 hPa).

In general, the relative heights of the convective outflow for the different models do not change significantly with geographical location, with the exception of TOMCAT and pTOMCAT which have significantly higher outflow heights for WA compared to all other regions. CATT-BRAMS and pTOMCAT_tropical have the highest outflow heights (150 hPa, ∼14 km for the MC region), and although the cloud top height analysis in Fig. 9. of R_2011 does not point to them as having the highest percentage of high clouds, this apparent discrepancy can be explained by the

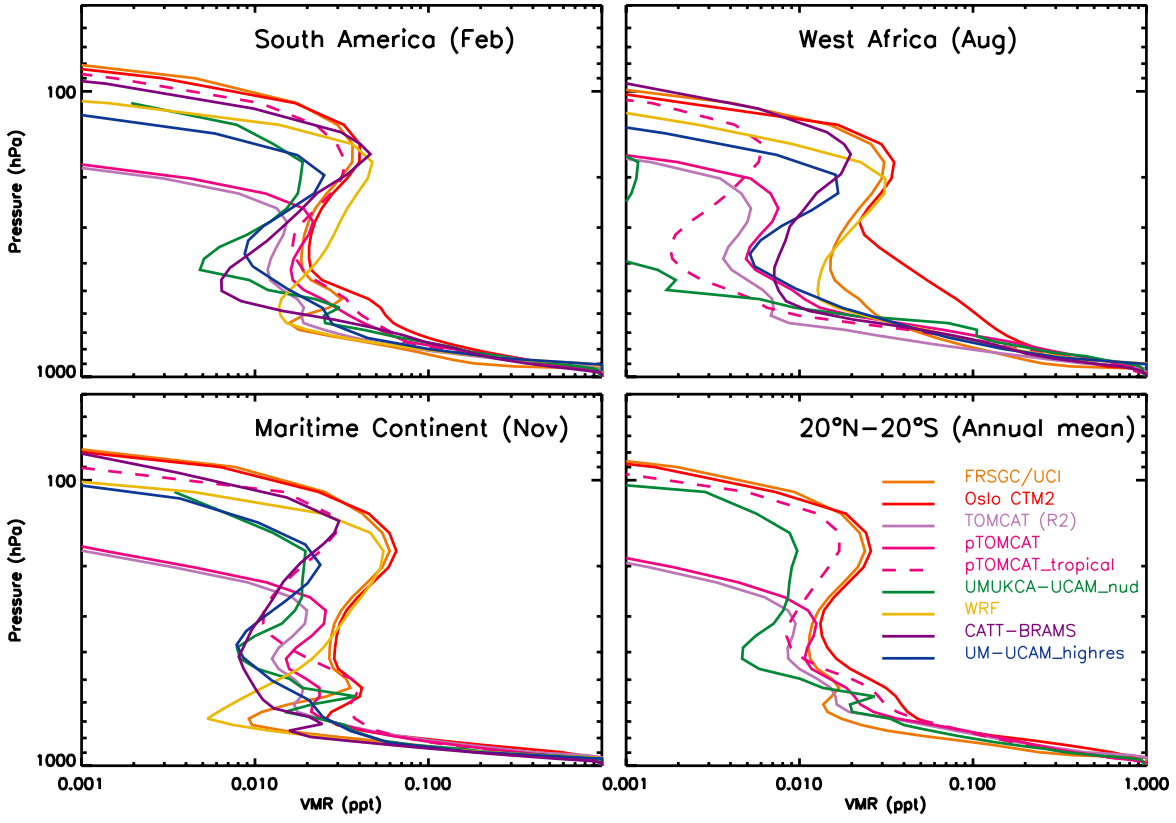

Fig. 2. The mean profile of T6h volume mixing ratios, for each model, averaged over three different areas for particular months of 2005, as well as an annual mean for the tropical region (lower right panel).

fact that both these models have convective detrainment at the top of the cloud rather than throughout the column. FRSGC/UCI, Oslo CTM2, WRF, UMUKCA-UCAM_nud and UM-UCAM_highres have fairly similar convective outflow heights for all regions (in the range 170–200 hPa (∼13–12 km), with FRSGC/UCI, Oslo CTM2 and WRF being slightly higher for some regions compared to the two UCAM models. The cloud top analysis in R_2011 shows that the cloud top distributions are highest for FRSGC/UCI, Oslo CTM2, and UMUKCA-UCAM_nud, and slightly lower for WRF and UM-UCAM_highres. In this case, the inconsistency between the high cloud tops produced by UMUKCA-UCAM_nud and the relatively lower convective outflow height can be attributed to the fact that the cloud fraction within the large model gridbox (3.7° × 2.5°) starts decreasing with height above ∼13 km. Despite having one of the lowest convective cloud top height distributions, over WA, UM-UCAM_highres has a relatively high convective outflow, similar in altitude (although greater in magnitude) to UMUKCA-UCAM_nud. Over WA and SA, WRF shows slightly lower outflow heights than Oslo CTM2 and FRSGC/UCI, and this is related to the distribution of the cloud top heights shown in Fig. 9 of R_2011, where WRF indeed has lower cloud top heights in these two regions than Oslo CTM2 and FRSGC/UCI, but very similar values over the MC, where the tracer outflow height is also similar.

We now analyse the tracer mixing ratio at the convective outflow in Fig. 2 and how it varies between models and between different geographical locations compared to the tropical mean. Generally FRSGC/UCI, Oslo CTM2 and WRF have the largest mixing ratios at the level of convective outflow, while TOMCAT and/or UMUKCA-UCAM_nud have the lowest. The other models predict mixing ratios between these extremes. The profiles from UM-UCAM_highres and UMUKCA-UCAM_nud are similar in all regions except WA, where the high resolution version of the model produces both a larger, and a higher altitude peak in tracer concentrations than the nudged model. Over SA, the nudged model has a much more pronounced mid-tropospheric minimum than UM-UCAM_highres. The very low monthly-mean tracer mixing ratio produced by UMUKCA-UCAM_nud for WA results from an anomalously low number of convective events for this region compared to other regions. Further investigation and additional model analysis showed that this underestimation of convection over the West Africa region is due to a problem with the interactive soil scheme used in the model.

For this region, the interactive soil scheme leads to underestimation of the soil moisture compared to soil climatologies (e.g. Willmott et al., 1985), and this in turn leads to a reduction of low-level moisture and convective activity.

Using the monthly mean precipitation rates shown in Fig. 6 of R_2011as a proxy for convective strength, it is difficult to explain the differences between the models. While Oslo CTM2 and FRSGC/UCI have one of the weakest precipitation rates among the models (in agreement with measurements), the outflow mixing ratios of the T6h tracer are the highest. WRF has comparatively high precipitation rates, and a similar tracer outflow concentration to Oslo CTM2 and FRSGC/UCI, however TOMCAT/pTOMCAT have rather high precipitation rates, and comparatively low peak tracer mixing ratios at the outflow level. The picture is more consistent over WA, where the high outflow mixing ratios of CATT-BRAMS, WRF and UM-UCAM_highres correspond with higher precipitation rates (Fig. 5 of R_2011), however Oslo CTM2 and FRSGC/UCI still have high outflow concentrations, despite having the lowest precipitation rates among the models.

Comparing the tracer mixing ratios at the outflow height between the different regions shows that for the Tropics, the tracer mixing ratios at the convective outflow height vary within the range 0.9–2.5 % of the mixing ratio imposed at the surface. These values are generally smaller compared to mixing ratios at the convective outflow for the three different domains, which show mixing ratios in the range 1.4–5 %, 0.5–3.5 %, and 1–7 % for SA, WA, and MC respectively (note that for WA we have ignored the anomalously low value associated to UMUKCA-UCAM_nud). The generally larger mixing ratios for these regions suggests that for most models under investigation, convective transport from the surface to the convective outflow height level is more efficient in these three regions at the selected times compared to the annual average convective transport in the whole tropical region. One exception is West Africa: for this region TOMCAT, pTOMCAT, pTOMCAT_tropical and UMUKCA-UCAM_nud have smaller mixing ratios at the convective outflow than they have for the Tropics.

While convection lifts the T6h tracer typically only to its convective outflow height, differences in the outflow height and in the tracer mixing ratio at this level will also have an impact on the amount of surface species which are subsequently transported upward from the TTL to the lower stratosphere.

The data in Fig. 2 can also be viewed as a time series, as shown in Fig. 3. Due to the short lifetime of T6h, a marked diurnal cycle, associated with convective development and decay, is observed in the upper tropospheric mixing ratios, and indeed, there is a marked periodicity in the T6h mixing ratios for all the models. Differences in both the altitude of the main convective outflow, as well as the strength of the vertical transport are obvious. A surprising difference, considering that most models use the same meteorological forcing data, is found in the timing and relative strength of the vertical transport.

The FRSGC/UCI and Oslo CTM2 produce similar time series, differing from pTOMCAT and TOMCAT (R2) data mainly by the mixing ratio, and altitude. At the very beginning of the time series, both FRSGC/UCI and Oslo CTM2 show moderate transport to higher levels, while pTOMCAT and TOMCAT (R2) show very little vertical transport in this period, although the diurnal cycle peaks at similar times. The inclusion of mid-level convection and generally enhanced convection in pTOMCAT_tropical leads to clearly higher tracer mixing ratios at 500–600 hPa, as well as much higher outflow heights in the upper troposphere, highlighting the importance of the convective parameterisation on tracer distributions. The increased resolution of pTOMCAT_T106, on the other hand, has little effect, when compared with the pTOMCAT results (see Feng et al., 2011 for further discussion). Although the time resolution of the input meteorological data, as well as the calculation method for the horizontal winds, differs for the TOMCAT models and, for example Oslo CTM2 (see Sect. 2), the modification of the convective scheme in pTOMCAT_tropical leads to results which are much more similar to Oslo CTM2 than the original pTOMCAT configuration.

UMUKCA-UCAM_nud shows greater transport to about 200hPa at days 305–308, a feature which is not seen in the TOMCAT (R2) or pTOMCAT plots. The lower convective activity around day 320 is seen in all of the models, however it starts 1–2 days earlier for TOMCAT (R2), pTOMCAT and UMUKCA-UCAM_nud than the other models. The free-running models produce generally similar results to the forced models. The timing of the enhanced concentrations in the upper troposphere differs slightly between UMUKCA-UCAM_nud and UM-UCAM_highres, for example around day 315.

The magnitude of the daily changes in vertical transport differs greatly between the models. CATT-BRAMS has the strongest daily cycle in convective activity, with T6h mixing ratios almost completely decaying to zero between consecutive peaks due to convective uplift, indicating that upward transport is negligible in the evening and early morning. The other models have far less variability in the upper troposphere, as the amount of convective transport varies less during a 24 h period. UMUKCA-UCAM_nud produces fairly constant enhanced mixing ratios at about 700 hPa, while in CATT-BRAMS, Oslo CTM2 and FRSGC/UCI the lower tropospheric peak mixing ratios are much more variable.

The differences in tropospheric transport to the convective outflow height results in different transport from this level to the lower stratosphere, where differences between models increase further, as illustrated by the T20 mixing ratios shown in Fig. 4. While the maximum difference between the November mean mixing ratio over the Maritime Continent of two models (UMSLIMCAT and FRSGC/UCI) was about a factor of three at around 100 hPa, at 70 hPa it is more

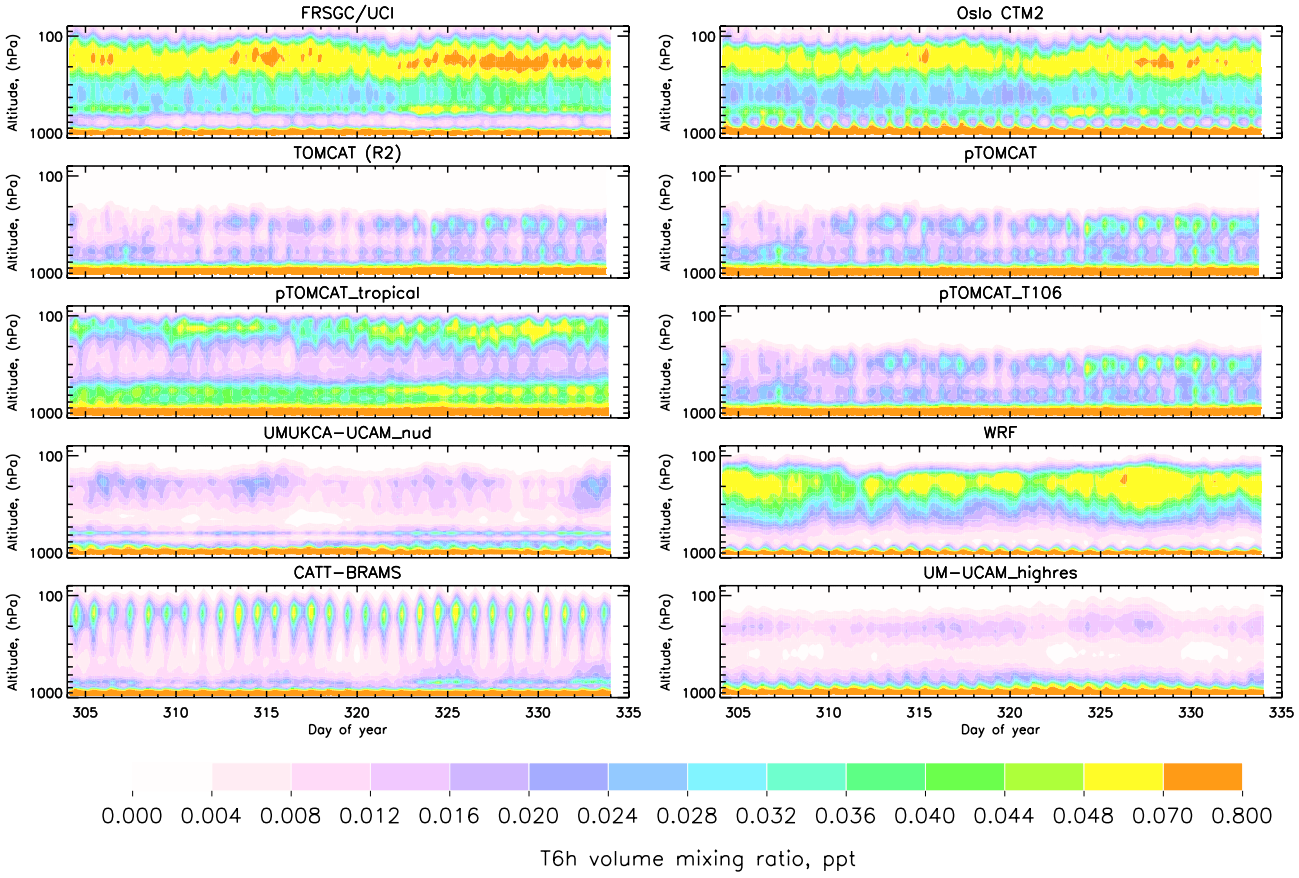

Fig. 3. Modelled profiles of mass mixing ratio as a function of time, for T6h, averaged over the Maritime Continent. The data runs from day 304 to 334, i.e. midnight on 1 November 2005 to midnight on 30 November 2005.

than an order of magnitude, and continues to increase with increasing altitude. There are two processes contributing to the divergence of the modelled mixing ratios, firstly the altitude at which the slow up-welling into the lower stratosphere begins, and secondly, the different rates of ascent provided by the models. For example, while the upper tropospheric peak in mixing ratios from UMCAM is lower than that of FRSGC/UCI over WA and SA, UMCAM has larger mixing ratios in the stratosphere, due to larger vertical transport within the lowermost stratosphere. On the other hand, in the tropical mean panel, FRSGC/UCI has greater mixing ratios in the upper troposphere than pTOMCAT, and the differences in mixing ratios continue to increase with altitude, due to a faster lower stratospheric up-welling in FRSGC/UCI than in pTOMCAT. However, the use of analysed divergence fields to calculate vertical transport in the TOMCAT/pTOMCAT model is known to overestimate the rate of vertical tracer transport, in comparison to the use of heating rates (Monge-Sanz et al., 2007; Hossaini et al., 2010).

In Fig. 4, the lowest tracer concentrations in the lower troposphere, except in West Africa, are those of TOMCAT_Louis. The TOMCAT (R2) and TOMCAT_Louis models differ in the boundary layer scheme, and it appears that the Louis scheme reduces the amount of tracer reaching the lower troposphere compared to the boundary layer scheme used in TOMCAT (R2). As described in Sect. 2.1, although both TOMCAT (R2) and TOMCAT_Louis contain the same convective parameterisation, the Louis BL mixing scheme produces a lower BL, less diffusion of tracers and no entrainment at the top of the BL, leading to less convective transport of tracers from the BL. This leads to significantly smaller mixing ratios for TOMCAT_Louis than TOMCAT (R2) up to about 100 hPa. The boundary layer mixing scheme therefore, has the potential to influence tracer mixing ratios throughout the troposphere.

+The profile for KASIMA starts at 600 hPa, as this is the lower boundary of the model. Due to the lack of a convective transport parameterisation, the profile of KASIMA shows no pronounced upper tropospheric peak, and has smaller mixing ratios than the profiles of the other models in the upper most troposphere and lowermost stratosphere.

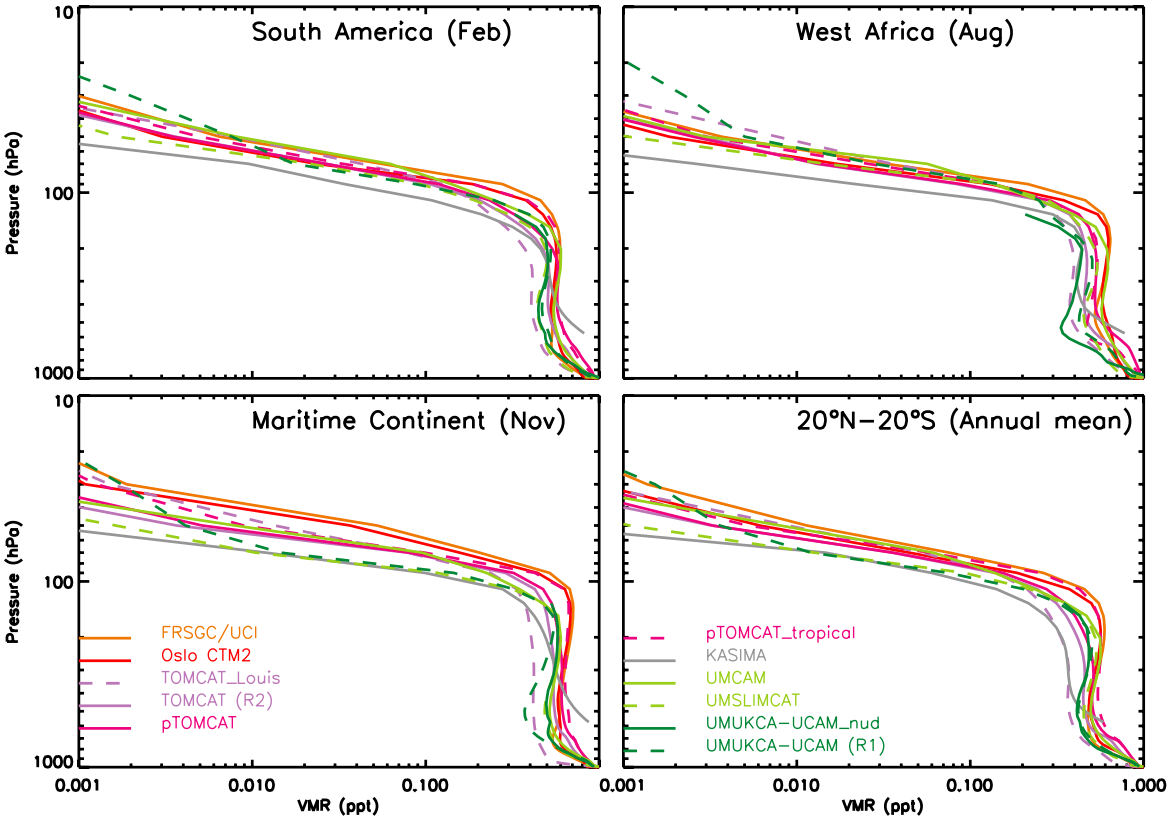

Fig. 4. The mean profile of T20 volume mixing ratios, for each model, averaged over three different areas for particular months of 2005, as well as an annual, tropical mean (lower right panel). The legend is split over the lower two panels, but refers to all four panels. No data were available for UMUKCA-UCAM_nud above 90 hPa.

The profiles from UMUKCA-UCAM_nud and UMUKCA-UCAM (R1) look very similar except over the MC, where the nudged version produces higher tracer mixing ratios in the middle troposphere, more in line with the results of the other models. Over WA, the situation is reversed, with the nudged version showing lower mixing ratios than all the other models between about 800 hPa and 400 hPa. By comparing Fig. 2 and Fig. 4, one can also note that the very large model differences in the vertical profiles for the extremely short lived T6h tracer are greatly reduced for the longer lived T20 tracer. Evidently, the lifetime of the tracer plays a role in how sensitive the details of the tracer distribution are to the differences in model transport.

5.2 Location of convection

The geographical location of convection is important as it determines the mixing ratios of water and the chemical species transported to the upper troposphere and the lower stratosphere. The idea of a "stratospheric fountain", with air preferentially entering the stratosphere over the western tropical Pacific and the Maritime Continent, was put forward by Newell and Gould-Stewart (1981). Subsequently Holton and Gettelman (2001) pointed out that the observed stratospheric water vapour mixing ratios could also be explained if air passed more or less horizontally though a cold area ("cold trap") in the upper troposphere, but did not necessarily enter the stratosphere at that location. Transport from the tropical boundary layer to the tropical tropopause layer and the stratosphere during January 2001 was investigated by Levine et al. (2007), who found that two thirds of the transport from the planetary boundary layer to the TTL occurs vertically over the Indian Ocean, Indonesia and the western Pacific. On the other hand, Ricaud et al. (2007) found that convective transport of trace gases into the lower most stratosphere mainly takes place above land convective regions, particularly Africa, in the season March-April-May.

The annual mean enhancement in T20 mixing ratio at approximately 200 hPa is shown in Fig. 5. This was calculated by dividing the annual mean T20 mixing ratio at each grid point by the annual, global mean mixing ratio on the 200 hPa level. The models generally agree on the location of the highest mixing ratios, although the magnitude of the tracer mixing ratios varies from model to model. The highest T20 mixing ratios are seen in the tropics, indicating that vertical transport to this level preferentially occurs there, as

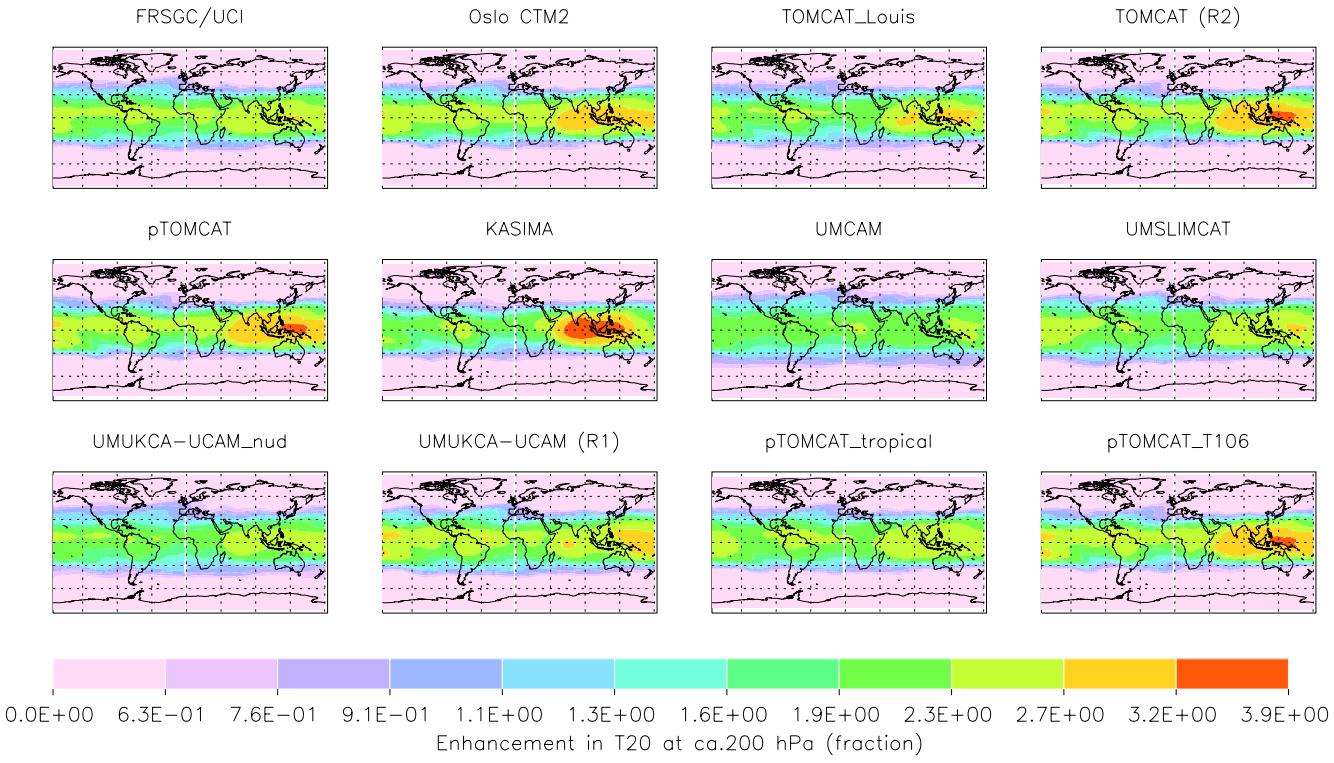

Fig. 5. The fraction enhancement of the 2005 annual mean mixing ratio of the T20 tracer, for each model, at the 200 hPa level. The enhancement was calculated by dividing the value at a particular point by the global mean at that level.

expected. The width of the band of high convective activity does not vary greatly between the models, and all models show the greatest vertical transport taking place over the western Pacific and Indian Ocean. Most of the models also show transport being slightly enhanced over South America and Africa. At 90 hPa (Fig. 6), the picture is similar, with most models indicating that the vast majority of the upward transport is taking place over the western Pacific and Indian Ocean, with very little contribution from other areas. FRSGC/UCI, Oslo CTM2, TOMCAT (R2) and pTOMCAT also show smaller contributions over South America and western Africa. No data were available at the 90 hPa level for UMUKCA-UCAM_nud. This general picture is also seen in Fig. 4 of R_2011, where maps of the annual mean precipitation rates are plotted. The measurement and re-analysis data shows high precipitation rates over the MC, Indian Ocean, across the Pacific, and to a lesser extent, over SA, and WA. TOMCAT and pTOMCAT greatly overestimate the measured precipitation rates, and have relatively high T20 mixing ratios at 200 hPa. pTOMCAT_tropical, also has high precipitation rates but has a comparatively low T20 mixing ratio at 200 hPa. At 90 hPa, however, the T20 mixing ratios of pTOMCAT_tropical, TOMCAT (R2) and PTOMCAT are similar, again illustrating the effect of the modified convective transport in pTOMCAT_tropical. Similarly, the precipitation rates for Oslo CTM2 and FRSGC/UCI are some of the smallest among the models, and while the mixing ratios of T20 for these models are also comparatively small at 200hPa, at 90 hPa the mixing ratios for Oslo CTM2 are the largest among the models. Again, while the model transport generally depends on the meteorological forcing data, the details of the models convective transport parameterisation have a large impact. At the 90 hPa level, the main difference between the models is the size of the T20 mixing ratio enhancement, related to the strength and depth of the convection, while the location of the highest mixing ratios is very consistent across all the models shown.

The seasonal cycle of the T20 mixing ratios at 90 hPa in the three areas SA, WA, MC as well as a tropical mean are shown in Fig. 7, which can be compared with the seasonal cycle of precipitation for the three study regions shown in Fig. 3 of R_2011. The 90 hPa level was chosen as it is located well into the TTL and is above the level of zero radiative heating. Tracers reaching this level will likely be transported into the lower stratosphere.

Over SA, most of the models show a seasonal variation with minima from about July to September and larger mixing ratios from about January to March. A similar pattern is seen over the MC with low values from about June to September and larger values in November and December. The mixing ratios over the MC are also generally larger than in the other areas, which leads to the general cycle over the MC being

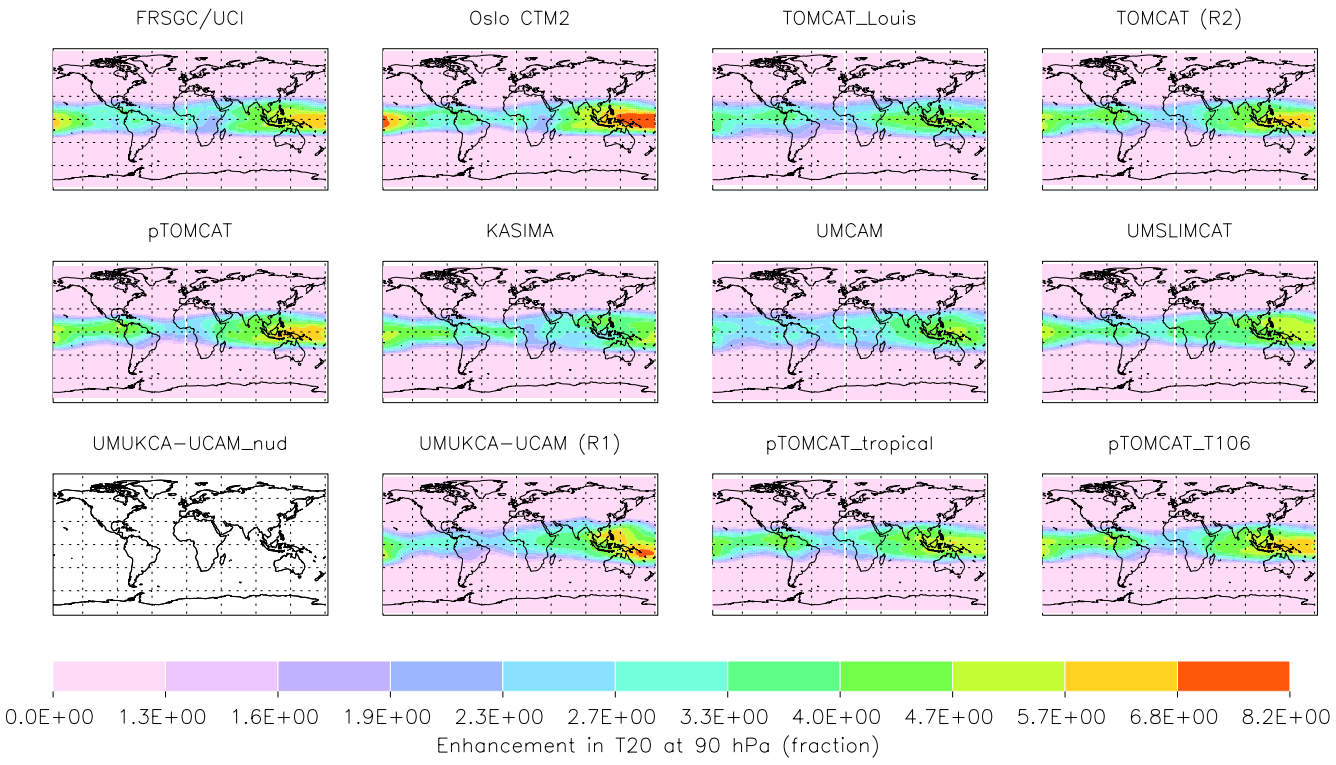

Fig. 6. The fraction enhancement of the 2005 annual mean mixing ratio of the T20 tracer, for each model at the 90 hPa level. No data was available at this level for UMUKCA-UCAM_nud. The enhancement was calculated by dividing the value at a particular point by the global mean at that level.

similar to that seen in the tropical mean. In contrast to the other models, UMSLIMCAT shows a peak in T20 concentration in August-September over the MC.

Over WA, few of the models show significant variation throughout the year, exceptions are UMCAM and UMUKCA-UCAM (R1), which both show larger mixing ratios towards the middle of the year. In the tropical average, mixing ratios are generally smaller from about July to October, and larger from November to May. For most of the models, the seasonal development of the tropical average shows a strong similarity to that over the MC, suggesting that the MC is the controlling region for the upper tropospheric tracer mixing ratios. In contrast, the mean tropical seasonal cycle for UMUKCA-UCAM (R1) shows a similarity with that over WA, with a peak in July–September.

If convection is the main control on tracer mixing ratios at 90 hPa in a particular region, the seasonal cycles in T20 mixing ratio shown in Fig. 7 should relate to the precipitation rates shown in Fig. 3 of R_2011. Over South America, all models show a marked seasonal cycle in precipitation rates, which is reflected in the T20 mixing ratios shown in Fig. 7. There is no direct relationship between amplitude of seasonal changes in the precipitation and amplitude of the seasonal changes in T20 for the different models, e.g. Oslo CTM2 and FRSGC/UCI have the highest amplitude changes in T20 mixing ratios and approximately the lowest amplitude change in precipitation rate. The situation is similar over the MC.

Over WA, there is also a seasonal cycle in precipitation rates, however, as described above, there is no pronounced seasonal cycle in T20 mixing ratios at 90 hPa for most of the models. The convective outflow heights shown in Fig. 2 are lower for WA than the MC and SA, and at 200 hPa (not shown), most of the models show a seasonal cycle over WA which correlates with the changes in precipitation throughout the year. The vertical transport from the surface to 90 hPa is therefore strongly linked to convection for the MC and SA but not for WA. Boundary layer tracers in the tropics are generally lofted convectively to a certain level (as shown in Fig. 2), and above that level large-scale transport processes are responsible for the further vertical transport. In WA, the tracer mixing ratios at higher levels in the models are controlled to a greater extent by large-scale transport processes. This corresponds well with observations carried out during the AMMA (African Monsoon Multidisciplinary Analyses) campaign during July and August 2006. Aircraft based measurements of several gas species were used to show the main convective outflow to be around 200 hPa in this region, and on certain days up to 100 hPa (Law et al., 2010; Fierli et al., 2011). Satellite based measurements of CO during the

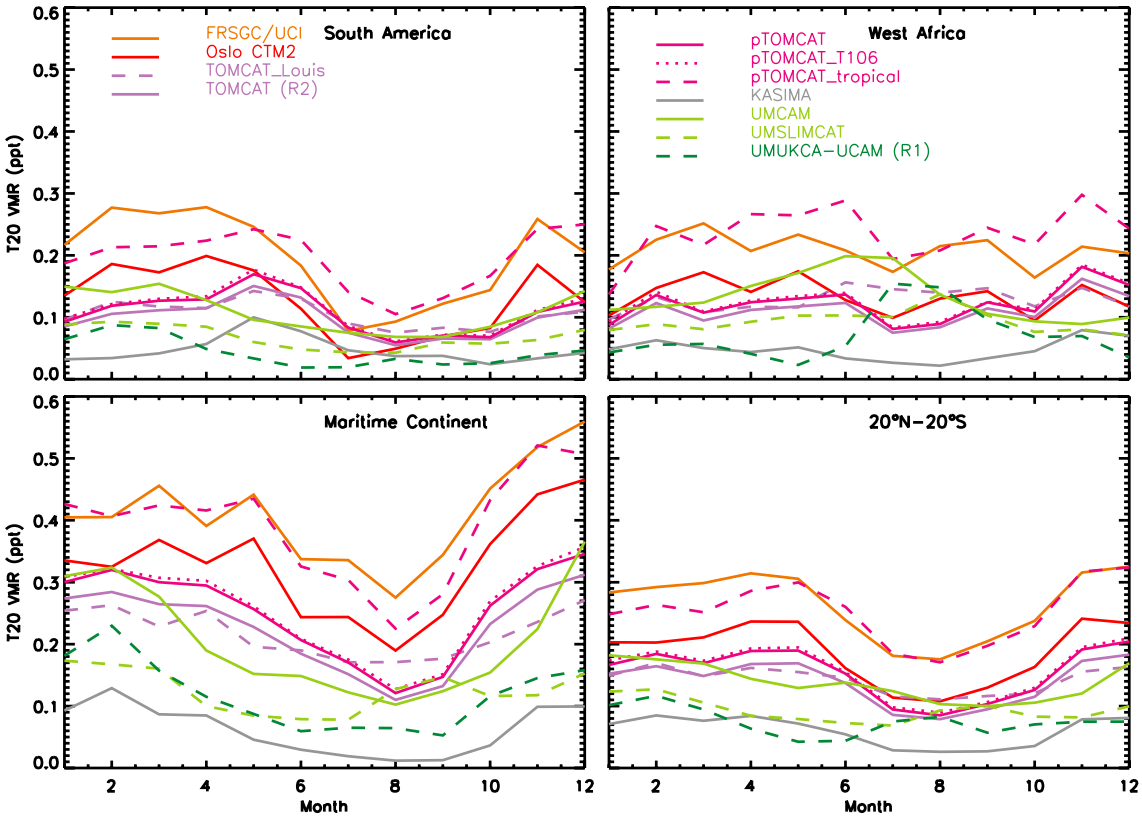

Fig. 7. The variation throughout 2005 of the T20 mixing ratio in the different models at 90 hPa over SA, WA, the MC and as a tropical mean. The legend is split over the two upper panels, but applies to all panels.

same time period show a convective influence up to around 220 hPa, with CO distributions above 150 hPa being controlled by large-scale transport (Barret et al., 2008).

5.3 Comparison with measurements

The idealised CO tracer used in the models has a uniform removal rate and no additional sources, therefore it cannot be expected to exactly reproduce the observed CO data on a particular day. It can still be used however, to evaluate general features of the model transport, such as the representation of seasonal cycles or the strength and altitude of the transport of lower tropospheric air to the upper troposphere. Because of its relatively long photochemical lifetime (i.e. ca. 1–3 months), the vertical distribution of CO is determined to a large extent by transport processes, although there is also a significant atmospheric source, due to the oxidation of hydrocarbons and methane (e.g. Shindell et al., 2006).

The modelled idealised CO fields were interpolated to the measurement times and locations along the flight track of the Geophysica, and a comparison with the measured data is plotted in Fig. 8. One of the focuses of the SCOUT-O3 measurement campaign in Darwin was to measure air that had been affected by the strong convective systems ("Hector") which form over the Tiwi islands (Brunner et al., 2009). On 16 November, air in the outflow of a Hector was sampled. Air which was not affected by the convection was also sampled on another leg of the flight, leading to the two branches of the measurement with substantially different mixing ratios. On 23 November the quiescent TTL was sampled, and on 25 November only weak convection was observed. On 30 November, relatively strong convection influenced the sampled air masses.

In general, all the models produce idealised CO values which are similar to the measured values. On 16 November, UMUKCA-UCAM_nud underestimates the measured CO mixing ratio in the lower-mid troposphere, while at about 350 hPa, pTOMCAT overestimates the mixing ratios. Higher in the atmosphere, around 100 hPa, most of the models better reproduce the convectively perturbed CO values than the background values, with UMUKCA-UCAM_nud still returning the lowest mixing ratios, which are within the range of the measurements. None of the models has sufficient spatial resolution to reproduce the difference between the perturbed and non-perturbed measured values. On 30 November, again the models capture the UT/LS CO as well as the slope of the

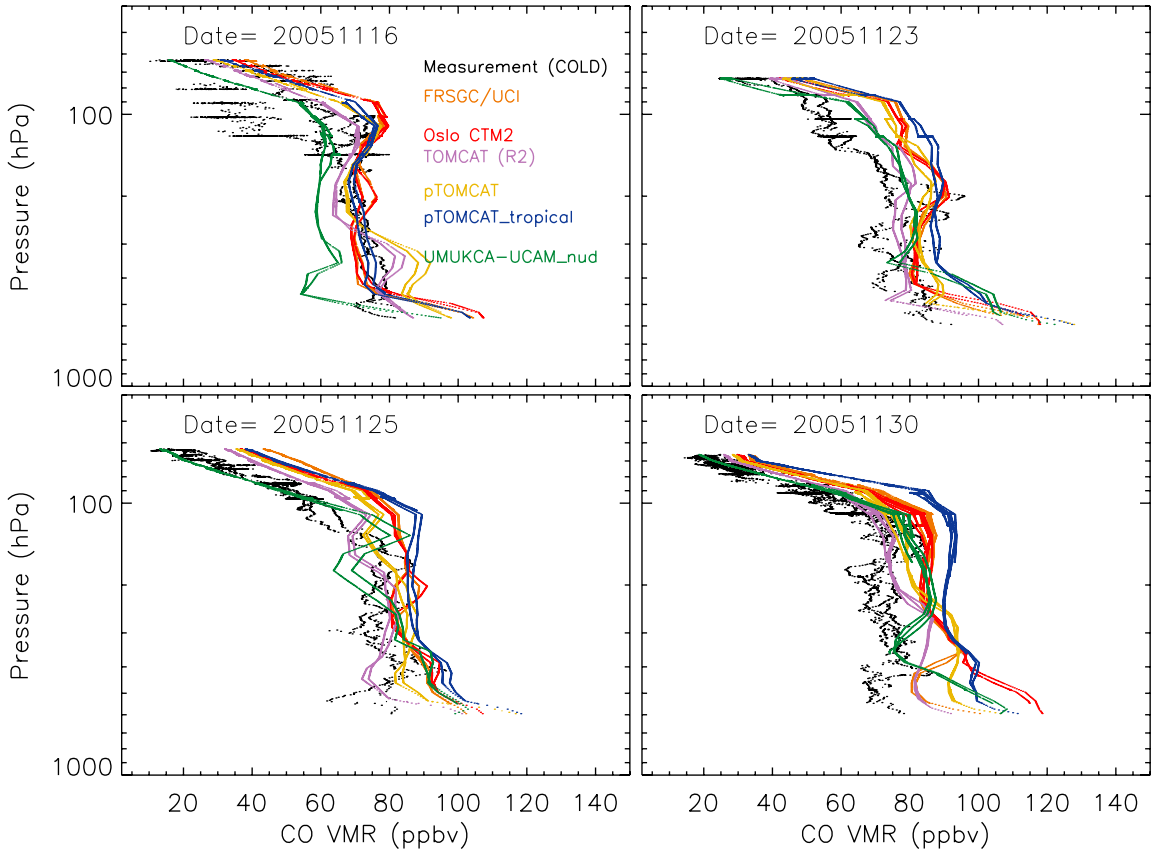

Fig. 8. A comparison between modelled and measured CO mixing ratios along the Geophysica flight track for 16, 23, 25 and 30 November 2005. The measurements were made during the SCOUT-O3 campaign in Darwin, Australia.

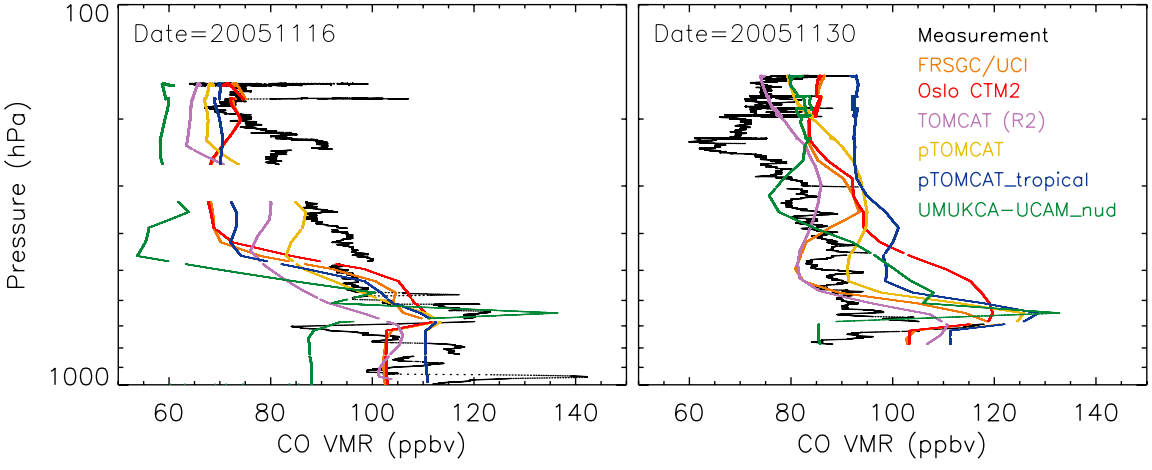

Fig. 9. A comparison between modelled and measured CO mixing ratios along the Egrett flight track for 16, and 30 November 2005. The measurements were made during the Active campaign in Darwin, Australia.

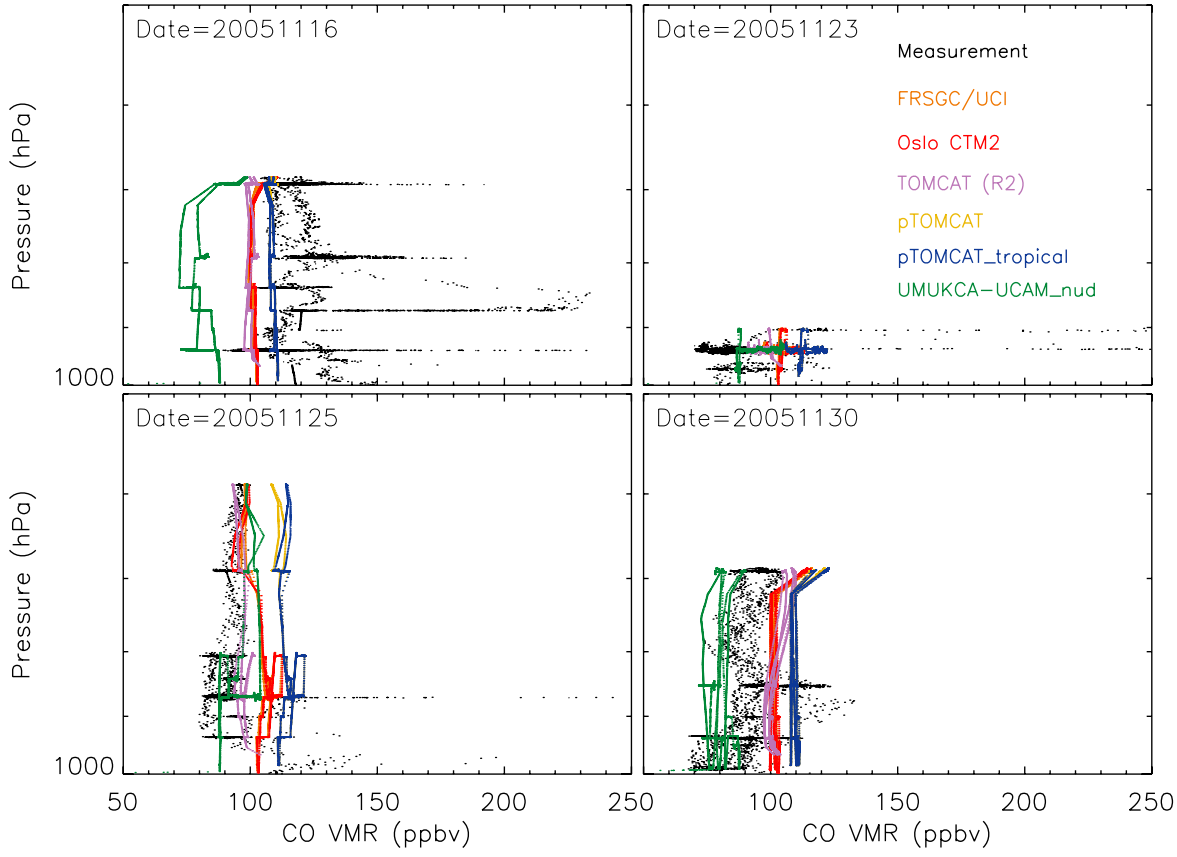

Fig. 10. A comparison between modelled and measured CO mixing ratios along the Dornier flight track for 16, 23, 25 and 30 November 2005. The measurements were made during the Active campaign in Darwin, Australia.

decay in mixing ratios with increasing altitude. In the lower troposphere, however, all models significantly overestimate the measured values.

On the less convectively active days, such as 23 November, the models capture the lower troposphere mixing ratios, however they all overestimate the values measured between about 150 hPa and 60 hPa, while on 25 November, the models generally reproduce the lower to mid tropospheric CO mixing ratios but, except for UMUKCA-UCAM_nud, overestimate the CO above 100 hPa. In general, the models all appear to have a vertical transport that corresponds more to convectively influenced profiles.

In order to investigate if the over or under estimated CO values are related to boundary layer CO in the models, Fig. 9 was created by interpolating the model data onto the flight track of the Egrett, on 16 and 30 November 2005. On 16 November, the air sampled by the Egrett contained higher CO mixing ratios than observed from the Geophysica, especially for convectively influenced air in the upper region of the profile. The models were, due to their resolution, unable to resolve these different air masses, and generally underestimate the Egrett-based measurements. The lower part of the profiles, below about 600 hPa, can be examined to determine if the surface CO mixing ratios may explain the model behaviour. In Fig. 9, on 16 November, most models have similar near-surface CO mixing ratios to those measured. UMUKCA-UCAM_nud has rather lower values, due to the larger grid including low CO air masses in the grid box average. This will contribute to the lower UMUKCA-UCAM_nud CO mixing ratios in the upper troposphere compared to the other models. Low level measurements (below 700 hPa) were also recorded by instrumentation on board the Dornier (Fig. 10). The Dornier carried out measurements both in air masses representative of the unperturbed background, and also targeted air which was influenced by localised biomass burning (Allen et al., 2008). The two kinds of measurements are clearly visible in the panels of Fig. 10, where the background CO values build the vertical column of measurements, and the biomass burning CO values form the horizontal layers with very high CO mixing ratios. At these lower tropospheric levels, the models all underestimate the average CO mixing ratios on 16 November (the horizontal sections of measurement data showing particularly high CO mixing ratios are where biomass burning

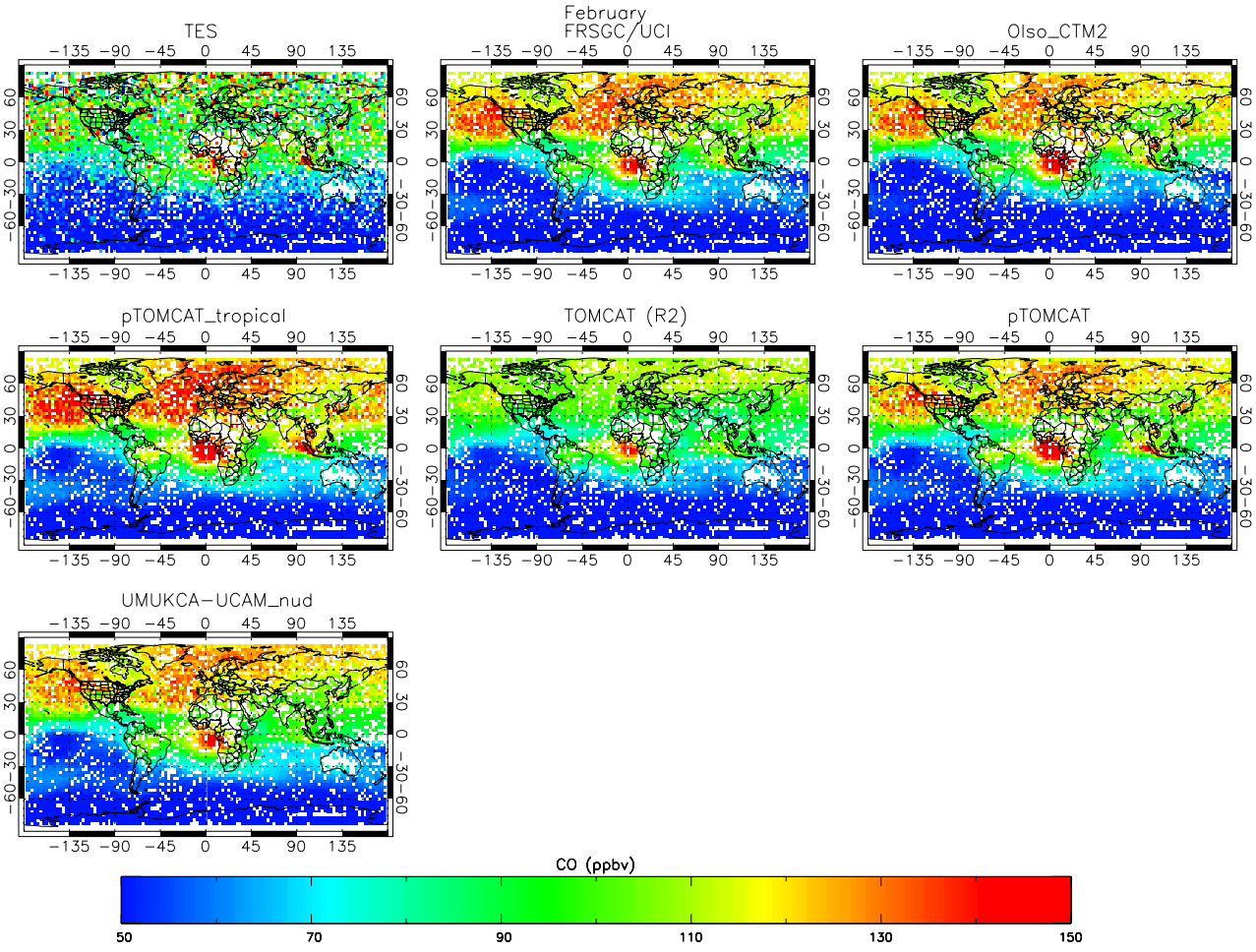

Fig. 11. A comparison between TES (Tropospheric Emission Spectrometer) satellite-based measurements of CO, and the monthly mean modelled CO mixing ratio at 350 hPa, for February 2005.

influenced air was sampled). The different aircraft measurements on 16 November show that there was a fair amount of spatial variability in the CO mixing ratios, on a scale which the models were not designed to resolve. On 23 November, Fig. 10 shows that most of the models slightly overestimate the average CO measurements near the surface (except UMUKCA-UCAM_nud), and while they do not have the resolution to resolve the magnitude of the CO enhancement in the biomass burning plumes which were observed, at approximately 920 hPa they do show a slight increase in CO mixing ratios. The Geophysica based measurements did not focus on convectively perturbed air on 23 November, therefore the overestimation of boundary layer CO by the models should not contribute to the overestimation higher in the troposphere.

On the 25 November, the measured CO mixing ratios very close to the surface were generally between 110 and 150 ppbv, rapidly decaying to average values of between approximately 80–100 ppbv above 900 hPa. The modelled values generally remain fairly constant with altitude below 600 hPa, overestimating CO above 900 hPa, and underestimating it below, with the exception of TOMCAT (R2) which matches the behaviour of the measurements very well. As only weak convection was observed on 25 November, it is not likely that the general overestimation of low level CO mixing ratios (above 900 hPa) in the models may explain the overestimation of the Geophysica based CO measurements at higher altitudes. Rather, as for 23 November, the vertical transport in the models is likely slightly too rapid under conditions with little convective activity. With its reduced convective transport compared to pTOMCAT_tropical, pTOMCAT does a notably better job of reproducing the decay of CO with height in Fig. 8, at least up to 100 hPa.

On 30 November, most of the models again have higher CO mixing ratios near the surface than were measured (Fig. 10), and as the measurements performed from the Geophysica and Egrett observed convectively influenced air, this low level overestimation may explain part of the high

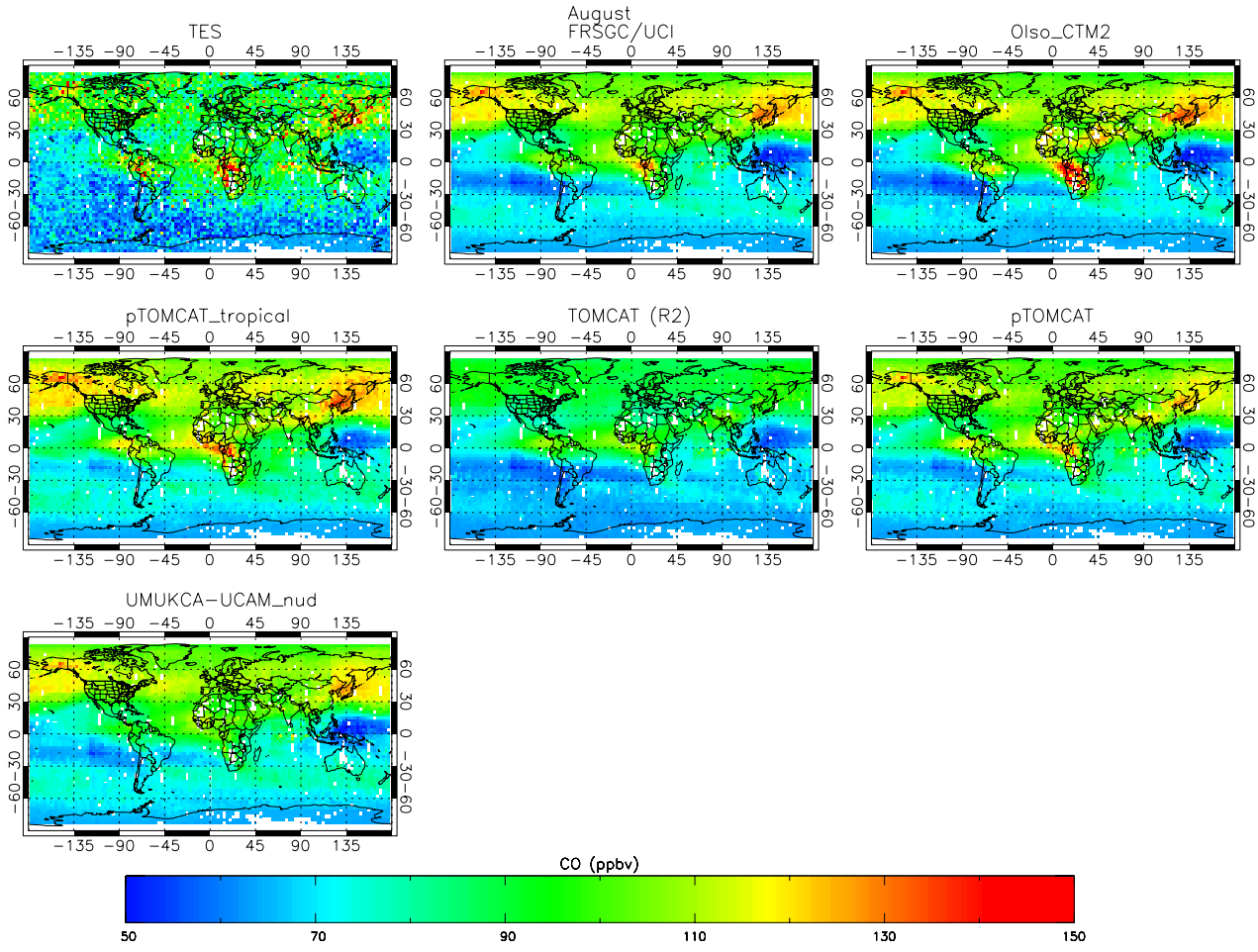

Fig. 12. As in Fig. 11, but for August 2005.

modelled values up to about 120 hPa (Figs. 8 and 9). However, even UMUKCA-UCAM_nud produced generally high values, especially around 200 hPa, despite underestimating the CO below 700 hPa. This gives further weight to the suggestion that a too rapid vertical transport is the cause of most of the overestimation.

There is a general pattern in Fig. 8, regarding which models have consistently higher CO mixing ratios than others, and it is interesting to note that this does not correlate with the cloud top height data presented in Fig. 9 of R_2011. There, pTOMCAT_tropical has clearly lower average cloud top heights over the MC during November than Oslo CTM2 or FRSGC/UCI, and UMUKCA-UCAM_nud even has the highest cloud tops, however UMUKCA-UCAM_nud has for the most part, the lowest CO mixing ratios along the profiles, and pTOMCAT_tropical the highest. This shows again that the tracer transport in the models does not depend solely on the depth of the convective transport, but also on how the entrainment and detrainment is parameterised. The lack of correlation with cloud top heights also suggests a significant role of non-convective vertical transport on determining the tracer profiles, for species with lifetimes of a few weeks or longer.

In general, the agreement of the models with the measurements throughout the troposphere is encouraging, however the vertical transport appears slightly too rapid. Furthermore, one should keep in mind that the differences between the models decrease as the lifetime of the tracer increases, and with a lifetime of between 1 and 3 months, depending on location and season (the lifetime is closer to 1 month in the tropics), CO can be considerably longer lived than halogen species with lifetimes of the order of days or weeks, such as bromoform (with a lifetime of about 30 days), although dibromomethane is actually much longer lived (with a lifetime of over 6 months, Hossaini et al., 2010).

The modelled monthly mean CO mixing ratios are compared with TES CO measurements at 350 hPa and 195 hPa, and for February, August and November 2005 in Figs. 11–16. In most cases, the models reproduce the seasonal large-scale features in the TES data, such as the interhemispheric gradients in concentration and the seasonal changes in the background CO concentration. In Fig. 11, however, all of the

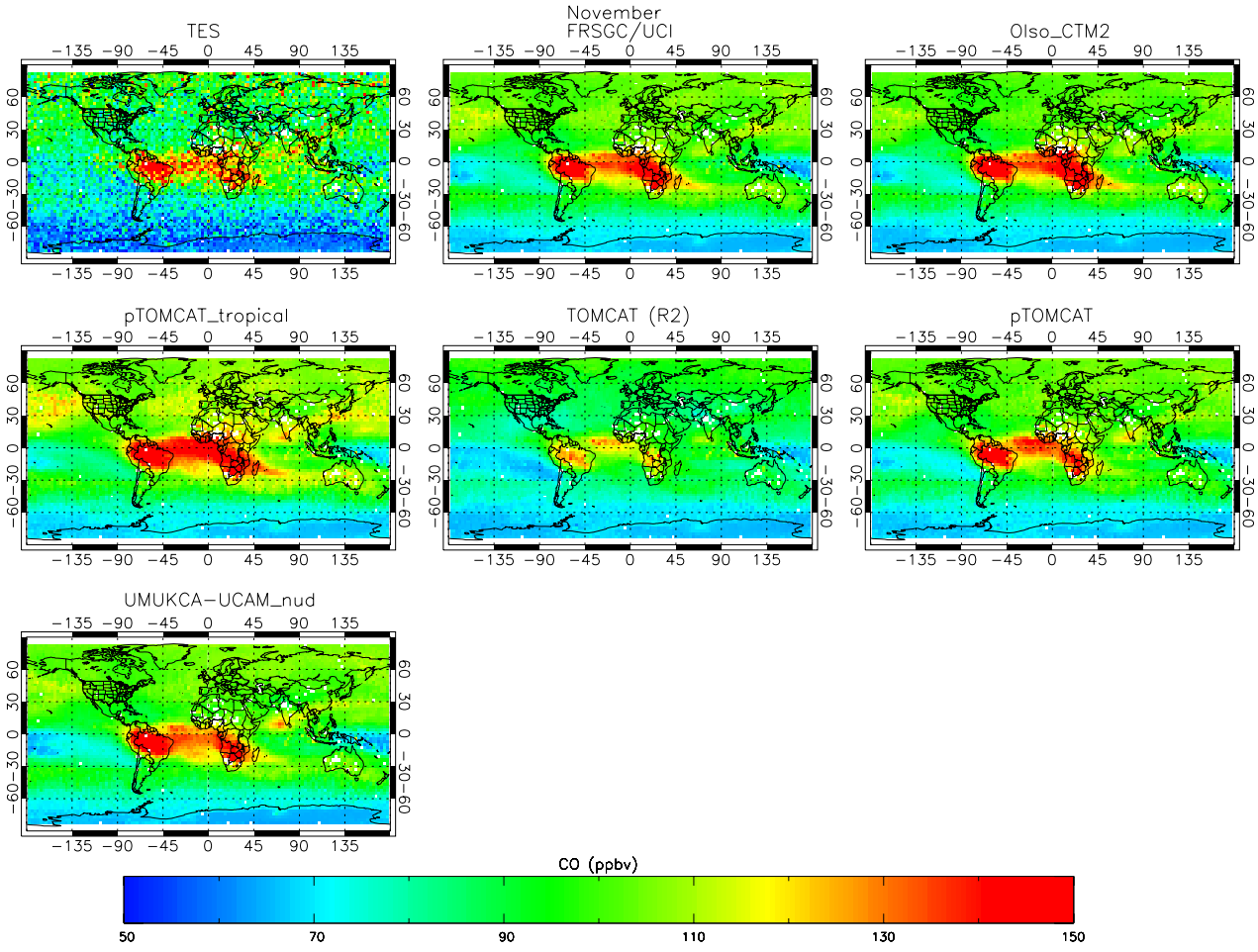

Fig. 13. As in Fig. 11, but for November 2005.

models except TOMCAT (R2) overestimate the background CO mixing ratios in the Northern Hemisphere, particularly north of 30° N. The plume of high CO values to the west of Africa is captured by all models, while the enhanced CO mixing ratios over Indonesia are reproduced by all models except TOMCAT (R2) and UMUKCA-UCAM_nud. This difference is due to the generally lower rate of vertical transport in TOMCAT (R2), and in the case of UMUKCA-UCAM_nud, due to the slightly coarser model resolution, which leads to lower peak surface CO values, and therefore a slightly reduced ability to reproduce high tracer concentrations over small areas. In August (Fig. 12), TES shows generally lower CO values, with enhanced mixing ratios west of Africa, and east of Asia. Most of the models reproduce this pattern, again with an overestimation of the background values (except for TOMCAT (R2)). While UMUKCA-UCAM_nud produces the higher CO mixing ratios east of Asia, the plume to the west of Africa is missing, and TOMCAT (R2) shows little sign of regional enhancements of CO mixing ratios. Also here, the generally more active transport of pTOMCAT_tropical is evident, leading to a greater overestimation of the background CO values than for pTOMCAT. In both Fig. 11 and Fig. 12, the general behaviour of the models is to produce too high background CO values. For small areas of high CO mixing ratios, the fact that the CO emissions are averaged over the model grid box leads to lower surface values, and therefore lower values higher in the troposphere (e.g. west of Africa in Fig. 12), however the larger areas of peak CO are well represented by most models. In Fig. 13, the high CO mixing ratios over Africa and South America are reproduced well by all models, with TOMCAT (R2) having comparatively low values and pTOMCAT_tropical again showing the highest values, as a result of the increased vertical transport. Again, all models overestimate the background CO values.

At 195 hPa, the models do a significantly better job of reproducing the measured background CO mixing ratios. The width of the tropical band of high CO mixing ratios is similar to the measurements in all cases. There are also smaller differences in the peak CO mixing ratios among the models, however as was the case at 350 hPa, pTOMCAT_tropical has the highest CO mixing ratios in the plume west of Africa, and

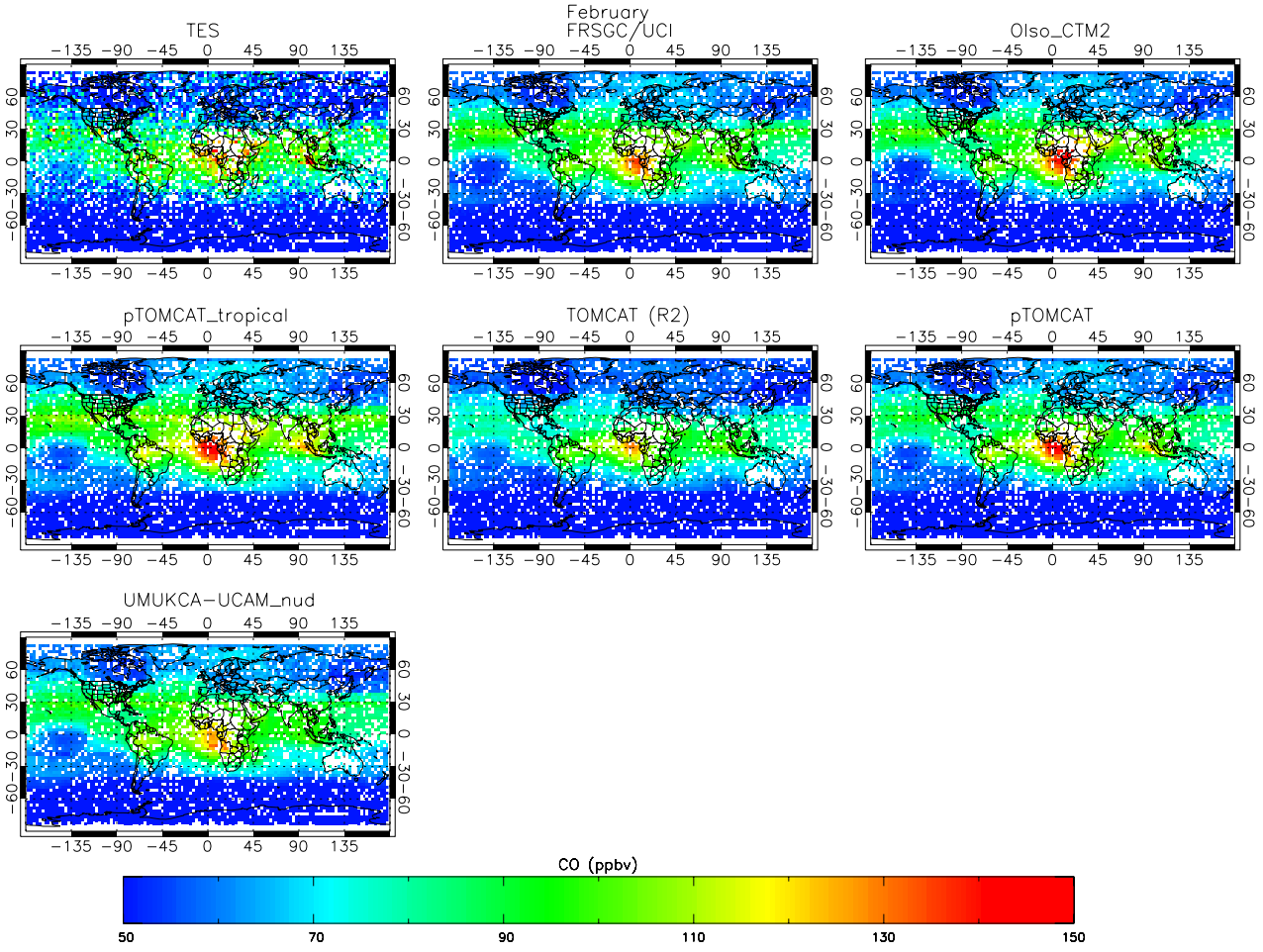

Fig. 14. As in Fig. 11, but for 195 hPa and February 2005.

TOMCAT (R2) has one of the lowest peak CO mixing ratios west of Africa. For August (Fig. 15) and November (Fig. 16), the situation is similar, with all models doing a reasonable job of reproducing the background and peak CO values. Comparing Figs. 11–16 with the annual mean precipitation rates shown in Fig. 4 of R_2011illustrates again that that the differences in the modelled tracer mixing ratios do not strictly depend on the meteorological fields. The annual mean precipitation rates are highest for TOMCAT (R2) and pTOMCAT, slightly lower for pTOMCAT_tropical, and those for Oslo CTM2/FRSGC/UCI and UMUKCA-UCAM_nud are similar (UMUKCA-UCAM_nud having the slightly higher precipitation rates). Despite this, both the peak, and background CO mixing ratios shown here are lowest for TOMCAT (R2). Oslo CTM2 and FRSGC/UCI have comparatively high values, similar to those of pTOMCAT, despite having far lower annual precipitation rates than pTOMCAT.

6 Discussion

For the offline models, i.e. those which use a pre-calculated set of meteorological forcing data, the short-lived tracer distribution is influenced to a large extent by the sub grid transport parameterisations in the model. The model differences are largest for the very short lived T6h, but are still observable for tracers such as CO, which have a much longer lifetime (ca. 1–3 months). Specifically, the choice of boundary layer mixing scheme has a large influence on the tropospheric tracer profile, as less dispersive schemes limit the flux of a tracer emitted at ground level into the free troposphere. When comparing the profiles from TOMCAT_Louis and TOMCAT_R2 in Fig. 4, the influence of the lower boundary layer heights and reduced mixing caused by the Louis (1979) boundary layer mixing scheme can be seen throughout the T20 tracer profile, up to at least 100 hPa. Similarly, pTOMCAT and pTOMCAT-tropical differ only in the calculation of convective transport. The large differences in the outflow height as illustrated by the T6h profiles shown in Fig. 2, as well as the differences in their CO profiles

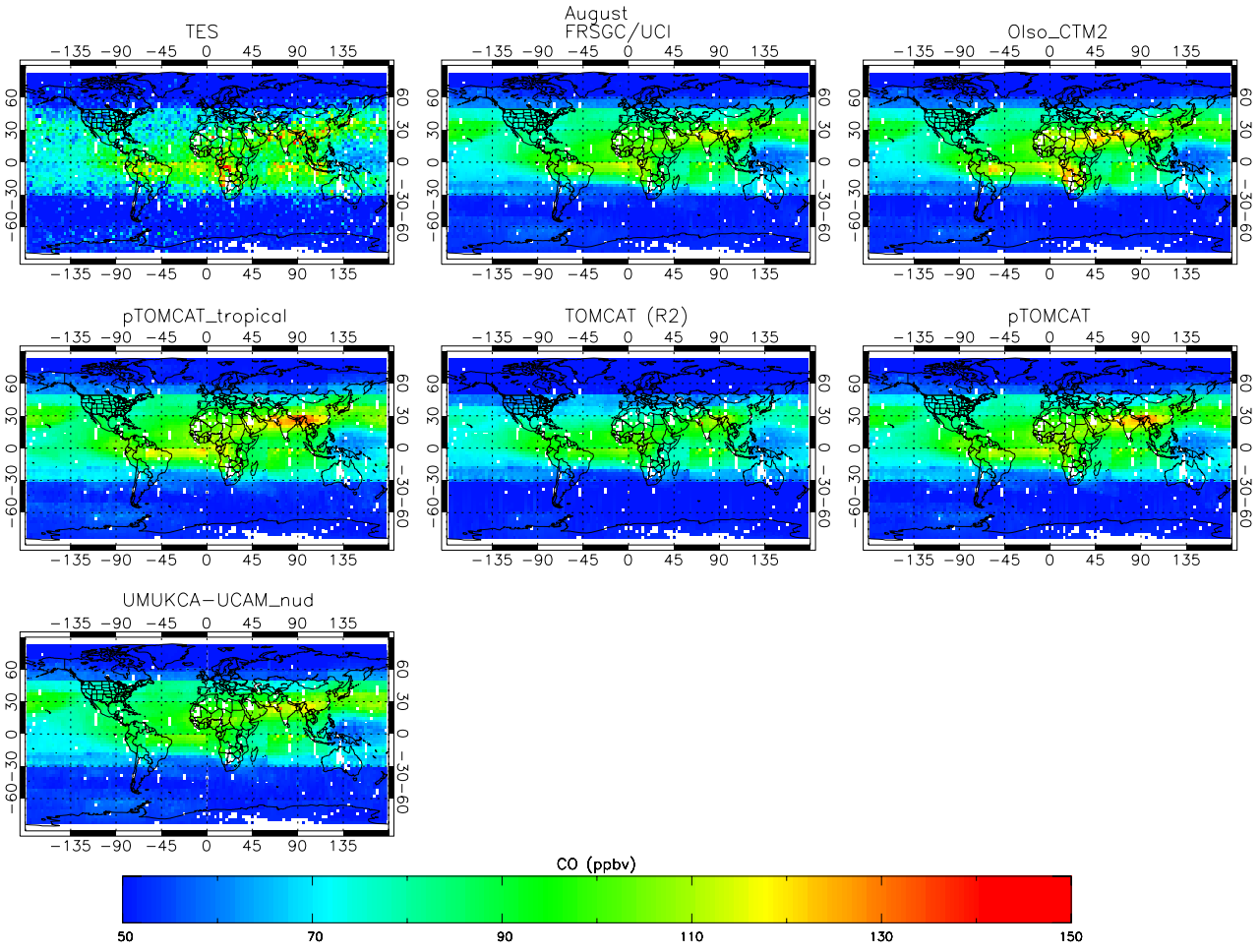

Fig. 15. As in Fig. 11, but for 195 hPa and August 2005.

again illustrate the significant influence of the convective parameterisation on vertical tracer transport. The only model which does not contain a convective transport parameterisation, KASIMA, also produced a tracer profile with smaller concentrations compared to other models up to 100 hPa. Over the middle portion of the tropical mean profile around 150 hPa–400 hPa, KASIMA and TOMCAT_Louis produced very similar T20 concentrations, smaller than the remaining models, further under-scoring the importance of the choice of boundary layer mixing scheme, and the use of an accurate convective transport parameterisation, when studying tropospheric tracer transport. The nudged version of UKCA (UMUKCA-UCAM_nud) shows significantly lower mixing ratios for the T6h tracer over parts of the profile for SA and WA, than is the case for the high resolution free running version (UM-UCAM_highres). Better agreement with other models is achieved with (UM-UCAM_highres). Despite the lack of an explicit boundary layer mixing scheme, UMSLIMCAT did not have a tropospheric tracer profile which was significantly different from that of the other models.

Although ECMWF meteorological data was used to drive all the offline models, there is around 100 hPa of difference in the altitude at which detrainment results in peak tracer concentrations, between several of the models. All aspects of the tracer distribution, i.e. the profile shape, the concentrations and the timing of transport events differ between several of the models which use the ECMWF data. This is in part due to the way in which vertical winds and convective activity are calculated from the ECMWF meteorological fields, as is shown by the large variability in precipitation rates among the models which was presented in R_2011, and from the differences in tracer profiles between pTOMCAT and pTOMCAT_tropical. However it was also shown that the modelled tracer profiles do not strictly correlate with proxies for convection, for example, despite particularly high precipitation rates, TOMCAT (R2) had one of the weakest convective vertical transports among the models tested. Clearly, despite the use of forcing data from the same source, the transport parameterisations implemented in the individual models play a substantial role in determining the tracer distribution.

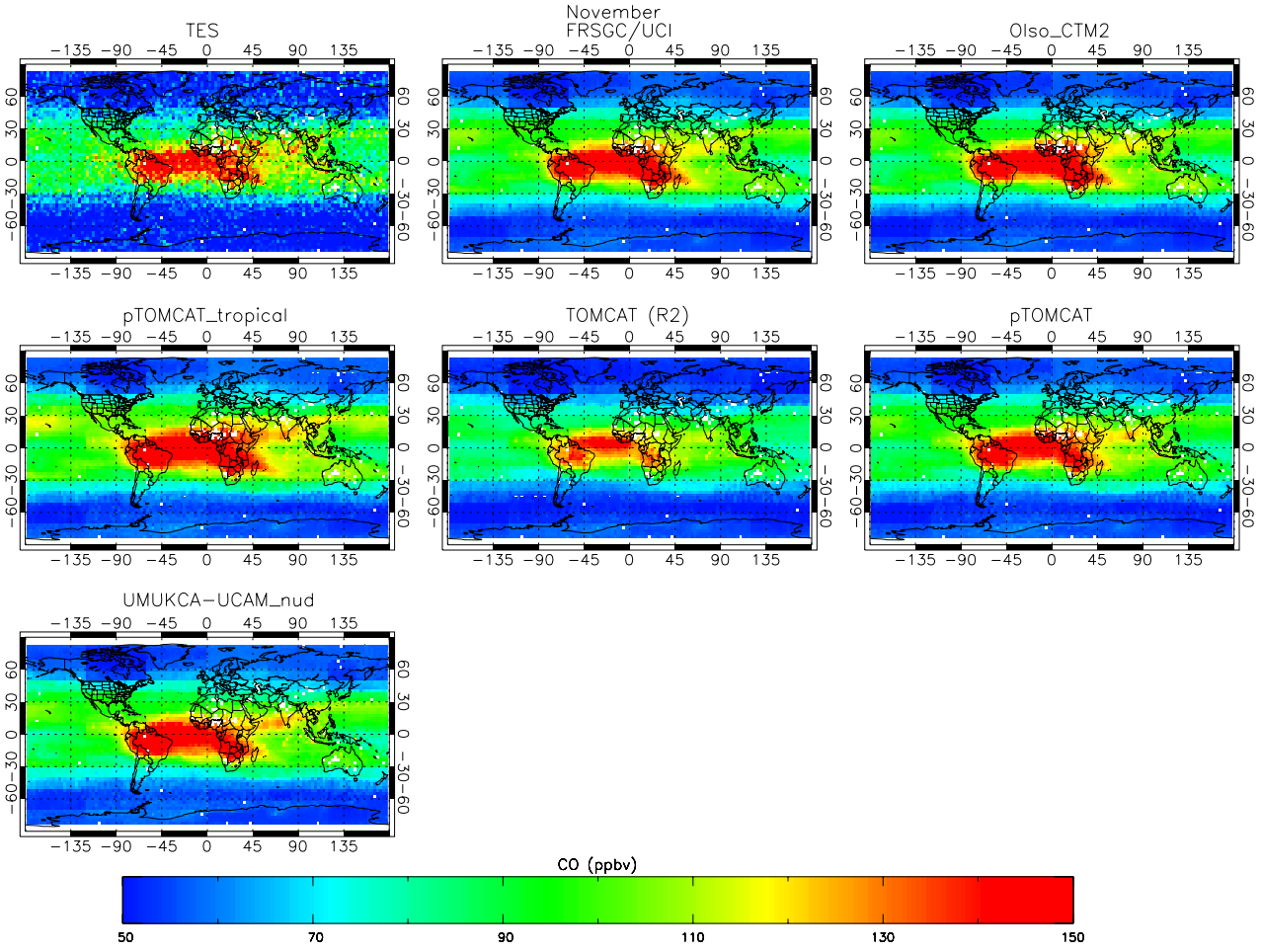

Fig. 16. As in Fig. 11, but for 195 hPa and November 2005.

All of the models included in Figs. 11–16 reproduced the general structure of the monthly differences in observed CO well, in comparison with the TES measurements, suggesting that the differences in model transport remain relatively constant throughout the year. All of the models except TOMCAT (R2) overestimate the background TES CO values at 350 hPa, suggesting a too rapid transport of CO away from the boundary layer, into the middle troposphere. TOMCAT (R2), however, represents the background TES CO values well. The coarser horizontal grid of UMUKCA-UCAM_nud in comparison to the other models leads to a greater reduction in peaks of surface CO mixing ratios, and does not allow the model to reproduce enhanced CO over small areas, such as Indonesia in Fig. 11, despite having similar background CO values to most of the other models. The tendency of most of the models to overestimate the observed CO profiles in Fig. 8 cannot be explained in all cases by too high surface mixing ratios, and therefore also points to a too rapid vertical transport.

For tracers with a lifetime of the order of a month, a priority should be for the model to reproduce the observed altitude at which tracer detrainment occurs. For shorter lived tracers, the intensity of the transport also becomes increasingly important.

The results presented here show that the timing of the transport events (on time scales of several days) is of lesser importance for average tracer mixing ratios in the UTLS, as in the long term the amount of tracer transported into the lower most stratosphere will not strongly depend on the timing of the events. On the other hand, if the diurnal timing of the transport events is linked to the stability of the boundary layer in the different models, this may create a systematic difference in the amount of tracer transported upwards, as the stability of the boundary layer affects the emission strength of PBL tracers into the free troposphere. For the composition of air entering the lowermost stratosphere, Figs. 2 and 4 show that the combination of convective detrainment height and vertical advection rate in the UT/LS is important. Models with a low convective detrainment altitude may still have larger mixing ratios of CO, for example, in the lowermost

stratosphere, because of a more rapid advection above the convective outflow.

The impact of differences in the strength of convection and detrainment altitude of convection between the models depends on the lifetime of the tracer and the altitude of interest. Throughout the troposphere, the modelled profiles of all tracers differed among the models, however, for altitudes of 100 hPa and higher, the idealised CO tracer profiles from all models were similar. For the shorter-lived tracers T20 and T6h, large differences in concentration at these altitudes were found, and it also became clear that tracer distributions throughout the troposphere become progressively more sensitive to differences in the models' transport schemes for shorter tracer lifetime, with the differences in the modelled tracer profiles being much larger for T6h than T20 or CO.

Although in this pair of papers we have focused on the representation of tropical deep convection in models, observations and modelling studies show that significant transport from the lower to the upper troposphere and the stratosphere also occurs at higher latitudes, for example during the Asian summer monsoon, where enhanced mixing ratios of lower tropospheric pollutants are found in the upper troposphere in an area over Asia and India, centred around 30° N (Li et al., 2005; Randel and Park, 2006; Park et al., 2007; Randel et al., 2010). The representation of these transport pathways in atmospheric models should be further evaluated in the future.

During the course of this study, it became clear that there is a need for measurements of tracers with which model transport can be validated, independently of model chemistry. Such a tracer should have relatively well defined emissions at the surface, be insoluble, and have a short lifetime via a loss process which is independent of other atmospheric species and of altitude. The only tracer which really fits this profile is radon. Although radon has been used in several studies in the past (e.g. Jacob et al., 1997), there is no extensive data set suitable for model evaluation. Despite the difficulties in measuring radon in the atmosphere (Kritz et al., 1998), the feasibility of large-scale measurements of radon throughout the atmosphere should be considered in the future – such a dataset would improve the existing possibilities for model validation enormously.

Acknowledgements. This work was supported with funding from the EU project SCOUT-O3. CRH was partly funded by SNSF grant number 200021_120175/1. NRPH thanks NERC for their Advanced Research Fellowship. NADR is funded via NERC NCEO. The CATT-BRAMS work was supported by the program LEFE/INSU in France (projects UTLS-tropicale and Tropopause 2009) and was performed using HPC resources of CINES under the allocation 2008-c2008012536 and 2009-c2009015036 made by GENCI (Grand Equipement National de Calcul Intensif). PJT was supported by NCEO (UK). We also thank NERC for funding the ACTIVE project and the NERC Airborne Research and Survey Facility (ARSF) for operational support of the Dornier-228 aircraft. Furthermore, the ACTIVE and SCOUT-O3 Tropical campaigns would not have been possible without the extensive support of the Australian Bureau of Meteorology, in particular Peter May at the Bureau of Meteorology Research Centre, Melbourne and Lori Chappel at the Regional Forecasting Centre in Darwin. We also thank the RAAF base, Darwin, for hosting the aircraft and campaign base, and for their logistical support.

Edited by: G. Vaughan

References

Allen, G., Vaughan, G., Bower, K. N., Williams, P. I., Crosier, J., Flynn, M., Connolly, P., Hamilton, J. F., Lee, J. D., Saxton, J. E., Watson, N. M., Gallagher, M., Coe, H., Allan, J., Choularton, T. W., and Lewis, A. C.: Aerosol and trace-gas measurements in the Darwin area during the wet season, J. Geophys. Res., 113, D06306, doi:10.1029/2007JD008706, 2008.

Arteta, J., Marécal, V., and Rivière, E. D.: Regional modelling of tracer transport by tropical convection – Part 1: Sensitivity to convection parameterization, Atmos. Chem. Phys., 9, 7081–7100, doi:10.5194/acp-9-7081-2009, 2009a.

Arteta, J., Marécal, V., and Rivière, E. D.: Regional modelling of tracer transport by tropical convection – Part 2: Sensitivity to model resolutions, Atmos. Chem. Phys., 9, 7101–7114, doi:10.5194/acp-9-7101-2009, 2009b.

Barret, B., Ricaud, P., Mari, C., Attié, J.-L., Bousserez, N., Josse, B., Le Flochmoën, E., Livesey, N. J., Massart, S., Peuch, V.-H., Piacentini, A., Sauvage, B., Thouret, V., and Cammas, J.-P.: Transport pathways of CO in the African upper troposphere during the monsoon season: a study based upon the assimilation of spaceborne observations, Atmos. Chem. Phys., 8, 3231–3246, doi:10.5194/acp-8-3231-2008, 2008.

Barret, B., Williams, J. E., Bouarar, I., Yang, X., Josse, B., Law, K., Pham, M., Le Flochmoën, E., Liousse, C., Peuch, V. H., Carver, G. D., Pyle, J. A., Sauvage, B., van Velthoven, P., Schlager, H., Mari, C., and Cammas, J.-P.: Impact of West African Monsoon convective transport and lightning NO_x production upon the upper tropospheric composition: a multi-model study, Atmos. Chem. Phys., 10, 5719–5738, doi:10.5194/acp-10-5719-2010, 2010.

Barth, M. C., Kim, S.-W., Wang, C., Pickering, K. E., Ott, L. E., Stenchikov, G., Leriche, M., Cautenet, S., Pinty, J.-P., Barthe, Ch., Mari, C., Helsdon, J. H., Farley, R. D., Fridlind, A. M., Ackerman, A. S., Spiridonov, V., and Telenta, B.: Cloud-scale model intercomparison of chemical constituent transport in deep convection, Atmos. Chem. Phys., 7, 4709–4731, doi:10.5194/acp-7-4709-2007, 2007.

Beer, R., Glavich, T., and Rider, D.: Tropospheric emission spectrometer for the Earth Observing System's Aura Satellite, Appl. Optics, 40, 2356–2367, 2001.

Berntsen, T., Fuglestvedt, J., Myhre, G., Stordal, F., and Berglen, T.: Abatement of greenhouse gases: Does location matter?, Climatic Change, 74, 377–411, doi:10.1007/s10584-006-0433-4, 2006.

Brunner, D., Siegmund, P., May, P. T., Chappel, L., Schiller, C., Müller, R., Peter, T., Fueglistaler, S., MacKenzie, A. R., Fix, A., Schlager, H., Allen, G., Fjaeraa, A. M., Streibel, M., and Harris, N. R. P.: The SCOUT-O3 Darwin Aircraft Campaign: rationale and meteorology, Atmos. Chem. Phys., 9, 93–117, doi:10.5194/acp-9-93-2009, 2009.

Chipperfield, M. P.: New version of the TOMCAT/SLIMCAT offline chemical transport model: Intercomparison of stratospheric tracer experiments, Q. J. Roy. Meteorol. Soc., 132, 1179–1203, doi:10.1256/qj.05.51, 2006.

Corti, T., Luo, B. P., Peter, T., Vömel, H., and Fu, Q.: Mean radiative energy balance and vertical mass fluxes in the equatorial upper troposphere and lower stratosphere, Geophys. Res. Lett., 32, L06802, doi:10.1029/2004GL021889, 2005.

Davies, T., Cullen, M., Malcolm, A., Mawson, M., Staniforth, A., White, A., and Wood, N.: A new dynamical core for the Met Office's global and regional modelling of the atmosphere, Q. J. Roy. Meteorol. Soc., 131, 1759–1782, doi:10.1256/qj.04.101, 2005.

Deeter, M. N., Edwards, D. P., Gille, J. C., and Drummond, J. R.: Sensitivity of MOPITT observations to carbon monoxide in the lower troposphere, J. Geophys. Res., 112, D24306, doi:10.1029/2007JD008929, 2007.

Deng, A., Seaman, N., Hunter, G., and Stauffer, D.: Evaluation of interregional transport using the MM5-SCIPUFF system, J. Appl. Meteorol., 43, 1864–1886, 2004.

Doherty, R. M., Stevenson, D. S., Collins, W. J., and Sanderson, M. G.: Influence of convective transport on tropospheric ozone and its precursors in a chemistry-climate model, Atmos. Chem. Phys., 5, 3205–3218, doi:10.5194/acp-5-3205-2005, 2005.

Feng, W., Chipperfield, M. P., Dorf, M., Pfeilsticker, K., and Ricaud, P.: Mid-latitude ozone changes: studies with a 3-D CTM forced by ERA-40 analyses, Atmos. Chem. Phys., 7, 2357–2369, doi:10.5194/acp-7-2357-2007, 2007.

Feng, W., Chipperfield, M. P., Dhomse, S., Monge-Sanz, B. M., Yang, X., Zhang, K., and Ramonet, M.: Evaluation of cloud convection and tracer transport in a three-dimensional chemical transport model, Atmos. Chem. Phys., 11, 5783–5803, doi:10.5194/acp-11-5783-2011, 2011.

Fierli, F., Orlandi, E., Law, K. S., Cagnazzo, C., Cairo, F., Schiller, C., Borrmann, S., Di Donfrancesco, G., Ravegnani, F., and Volk, C. M.: Impact of deep convection in the tropical tropopause layer in West Africa: in-situ observations and mesoscale modelling, Atmos. Chem. Phys., 11, 201–214, doi:10.5194/acp-11-201-2011, 2011.

Folkins, I., Loewenstein, M., Podolske, J., Oltmans, S., and Proffitt, M.: A barrier to vertical mixing at 14 km in the tropics: Evidence from ozonesondes and aircraft measurements, J. Geophys. Res., 104, 22095–22102, 1999.

Folkins, I., Oltmans, S., and Thompson, A.: Tropical convective outflow and near surface equivalent potential temperatures, Geophys. Res. Lett., 27, 2549–2552, 2000.

Folkins, I., Bernath, P., Boone, C., Donner, L. J., Eldering, A., Lesins, G., Martin, R. V., Sinnhuber, B. M., and Walker, K.: Testing convective parameterizations with tropical measurements of HNO_3, CO, H_2O, and O_3^-: Implications for the water vapor budget, J. Geophys. Res., 111, D23304, doi:10.1029/2006JD007325, 2006.

Freitas, S. R., Longo, K. M., Silva Dias, M. A. F., Chatfield, R., Silva Dias, P., Artaxo, P., Andreae, M. O., Grell, G., Rodrigues, L. F., Fazenda, A., and Panetta, J.: The Coupled Aerosol and Tracer Transport model to the Brazilian developments on the Regional Atmospheric Modeling System (CATT-BRAMS) – Part 1: Model description and evaluation, Atmos. Chem. Phys., 9, 2843–2861, doi:10.5194/acp-9-2843-2009, 2009.

Fritsch, J. M. and Chappell, C. F.: Numerical prediction of convectively driven mesoscale pressure systems.1. Convective parameterization, J. Atmos. Sci., 37, 1722–1733, 1980.

Fueglistaler, S., Dessler, A. E., Dunkerton, T. J., Folkins, I., Fu, Q., and Mote, P. W.: Tropical Tropopause Layer, Rev. Geophys., 47, RG1004, doi:10.1029/2008RG000267, 2009.

Grant, A.: Cloud-base fluxes in the cumulus-capped boundary layer, Q. J. Roy. Meteorol. Soc., 127, 407–421, 2001.

Grant, A. and Brown, A.: A similarity hypothesis for shallow-cumulus transports, Q. J. Roy. Meteorol. Soc., 125, 1913–1936, 1999.

Gregory, D. and Rowntree, P. R.: A mass flux convection scheme with representation of cloud ensemble characteristics and stability-dependent closure, Mon. Weather Rev., 118, 1483–1506, 1990.

Gregory, A. and West, V.: The sensitivity of a model's stratospheric tape recorder to the choice of advection scheme, Q. J. Roy. Meteorol. Soc., 128, 1827–1846, 2002.

Grell, G. and Dévényi, D.: A generalized approach to parameterizing convection combining ensemble and data assimilation techniques, Geophys. Res. Lett., 29(14), 1693, doi:10.1029/2002GL015311, 2002.

Hartmann, D. L. and Larson, K.: An important constraint on tropical cloud - climate feedback, Geophys. Res. Lett., 29, 1951, doi:10.1029/2002GL015835, 2002.

Heyes, W. J., Vaughan, G., Allen, G., Volz-Thomas, A., Pätz, H.-W., and Busen, R.: Composition of the TTL over Darwin: local mixing or long-range transport?, Atmos. Chem. Phys., 9, 7725–7736, doi:10.5194/acp-9-7725-2009, 2009.

Holton, J. and Gettelman, A.: Horizontal transport and the dehydration of the stratosphere, Geophys. Res. Lett., 28, 2799–2802, 2001.

Holtslag, A. A. M. and Boville, B. A.: Local versus nonlocal boundary-layer diffusion in a global climate model, J. Climate, 6, 1825–1842, 1993.

Holtslag, A., Debruijn, E., and Pan, H.: A high-resolution air-mass transformation model for short-range weather forecasting, Mon. Weather Rev., 118, 1561–1575, 1990.

Hosking, J. S., Russo, M. R., Braesicke, P., and Pyle, J. A.: Modelling deep convection and its impacts on the tropical tropopause layer, Atmos. Chem. Phys., 10, 11175–11188, doi:10.5194/acp-10-11175-2010, 2010.

Hossaini, R., Chipperfield, M. P., Monge-Sanz, B. M., Richards, N. A. D., Atlas, E., and Blake, D. R.: Bromoform and dibromomethane in the tropics: a 3-D model study of chemistry and transport, Atmos. Chem. Phys., 10, 719–735, doi:10.5194/acp-10-719-2010, 2010.

Jacob, D., Prather, M., Rasch, P., Shia, R., Balkanski, Y., Beagley, S., Bergmann, D., Blackshear, W., Brown, M., Chiba, M., Chipperfield, M., deGrandpre, J., Dignon, J., Feichter, J., Genthon, C., Grose, W., Kasibhatla, P., Kohler, I., Kritz, M., Law, K., Penner, J., Ramonet, M., Reeves, C., Rotman, D., Stockwell, D., VanVelthoven, P., Verver, G., Wild, O., Yang, H., and Zimmermann, P.: Evaluation and intercomparison of global atmospheric transport models using Rn-222 and other short-lived tracers, J. Geophys. Res., 102, 5953–5970, 1997.

Janjic, Z.: The Step-Mountain ETA Coordinate model – further developments of the convection, viscous sublayer, and turbulence closure schemes, Mon. Weather Rev., 122, 927–945, 1994.

Janjic, Z.: Comments on "Development and evaluation of a con-

vection scheme for use in climate models", J. Atmos. Sci., 57, p. 3686, 2000.

Klemp, J. and Wilhelmson, R.: Simulation of 3-dimensional convective story dynamics, J. Atmos. Sci., 35, 1070–1096, 1978.

Kouker, W., Offermann, D., Kull, V., Reddmann, T., Ruhnke, R., and Franzen, A.: Streamers observed by the CRISTA experiment and simulated in the KASIMA model, J. Geophys. Res., 104, 16405–16418, 1999.

Kritz, M., Rosner, S., and Stockwell, D.: Validation of an offline three-dimensional chemical transport model using observed radon profiles – 1. Observations, J. Geophys. Res., 103, 8425–8432, 1998.

Kupper, C., Thuburn, J., Craig, G. C., and Birner, T.: Mass and water transport into the tropical stratosphere: A cloud-resolving simulation, J. Geophys. Res., 109, D10111, doi:10.1029/2004JD004541, 2004.

Laube, J. C., Engel, A., Bönisch, H., Möbius, T., Worton, D. R., Sturges, W. T., Grunow, K., and Schmidt, U.: Contribution of very short-lived organic substances to stratospheric chlorine and bromine in the tropics – a case study, Atmos. Chem. Phys., 8, 7325–7334, doi:10.5194/acp-8-7325-2008, 2008.

Law, K. S. and Sturges, W. T.: Halogenated very short-lived substances, in: WMO Scientific Assessment of Ozone Depletion 2006: Global ozone research and monitoring project, Rep. 50, World Meteorol. Org., Geneva, 2007.

Law, K. S., Fierli, F., Cairo, F., Schlager, H., Borrmann, S., Streibel, M., Real, E., Kunkel, D., Schiller, C., Ravegnani, F., Ulanovsky, A., D'Amato, F., Viciani, S., and Volk, C. M.: Air mass origins influencing TTL chemical composition over West Africa during 2006 summer monsoon, Atmos. Chem. Phys., 10, 10753–10770, doi:10.5194/acp-10-10753-2010, 2010.

Lawrence, M. and Rasch, P.: Tracer transport in deep convective updrafts: Plume ensemble versus bulk formulations, J. Atmos. Sci., 62, 2880–2894, 2005.

Lawrence, M., von Kuhlmann, R., Salzmann, M., and Rasch, P.: The balance of effects of deep convective mixing on tropospheric ozone, Geophys. Res. Lett., 30, 1940, doi:10.1029/2003GL017644, 2003.

Leonard, B. P., Lock, A. P., and Macvean, M. K.: The nirvana scheme applied to one-dimensional advection, International Journal of Numerical Methods for Heat & Fluid Flow, 5, 341–377, 1995.

Levine, J. G., Braesicke, P., Harris, N. R. P., Savage, N. H., and Pyle, J. A.: Pathways and timescales for troposphere-to-stratosphere transport via the tropical tropopause layer and their relevance for very short lived substances, J. Geophys. Res., 112, D04308, doi:10.1029/2005JD006940, 2007.

Li, Q., Jiang, J., Wu, D., Read, W., Livesey, N., Waters, J., Zhang, Y., Wang, B., Filipiak, M., Davis, C., Turquety, S., Wu, S., Park, R., Yantosca, R., and Jacob, D.: Convective outflow of South Asian pollution: A global CTM simulation compared with EOS MLS observations, Geophys. Res. Lett., 32, L14826, doi:10.1029/2005GL022762, 2005.

Liang, Q., Stolarski, R. S., Kawa, S. R., Nielsen, J. E., Douglass, A. R., Rodriguez, J. M., Blake, D. R., Atlas, E. L., and Ott, L. E.: Finding the missing stratospheric Br_y a global modeling study of $CHBr_3$ and CH_2Br_2, Atmos. Chem. Phys., 10, 2269–2286, doi:10.5194/acp-10-2269-2010, 2010.

Lock, A., Brown, A., Bush, M., Martin, G., and Smith, R.: A new boundary layer mixing scheme. Part I: Scheme description and single-column model tests, Mon. Weather Rev., 128, 3187–3199, 2000.

Lopez, J. P., Luo, M., Christensen, L. E., Loewenstein, M., Jost, H., Webster, C. R., and Osterman, G.: TES carbon monoxide validation during two AVE campaigns using the Argus and ALIAS instruments on NASA's WB-57F, J. Geophys. Res., 113, D16S47, doi:10.1029/2007JD008811, 2008.

Louis, J. F.: Parametric model of vertical eddy fluxes in the atmosphere, Bound.-Lay. Meteorol., 17, 187–202, 1979.

Luo, M., Rinsland, C., Fisher, B., Sachse, G., Diskin, G., Logan, J., Worden, H., Kulawik, S., Osterman, G., Eldering, A., Herman, R., and Shephard, M.: TES carbon monoxide validation with DACOM aircraft measurements during INTEX-B 2006, J. Geophys. Res., 112, D24S48, doi:10.1029/2007JD008803, 2007.

Mahowald, N., Rasch, P., and Prinn, R.: Cumulus parameterizations in chemical transport models, J. Geophys. Res., 100, 26173–26189, 1995.

Mellor, G. and Yamada, T.: Development of a turbulence closure-model for geophysical fluid problems, Rev. Geophys., 20, 851–875, 1982.

Monge-Sanz, B. M., Chipperfield, M. P., Simmons, A. J., and Uppala, S. M.: Mean age of air and transport in a CTM: Comparison of different ECMWF analyses, Geophys. Res. Lett., 34, L04801, doi:10.1029/2006GL028515, 2007.

Morgenstern, O., Braesicke, P., O'Connor, F. M., Bushell, A. C., Johnson, C. E., Osprey, S. M., and Pyle, J. A.: Evaluation of the new UKCA climate-composition model – Part 1: The stratosphere, Geosci. Model Dev., 2, 43–57, doi:10.5194/gmd-2-43-2009, 2009.

Mullendore, G. L., Homann, A. J., Bevers, K., and Schumacher, C.: Radar reflectivity as a proxy for convective mass transport, J. Geophys. Res., 114, D16103, doi:10.1029/2008JD011431, 2009.

Nassar, R., Logan, J. A., Worden, H. M., Megretskaia, I. A., Bowman, K. W., Osterman, G. B., Thompson, A. M., Tarasick, D. W., Austin, S., Claude, H., Dubey, M. K., Hocking, W. K., Johnson, B. J., Joseph, E., Merrill, J., Morris, G. A., Newchurch, M., Oltmans, S. J., Posny, F., Schmidlin, F. J., Voemel, H., Whiteman, D. N., and Witte, J. C.: Validation of Tropospheric Emission Spectrometer (TES) nadir ozone profiles using ozonesonde measurements, J. Geophys. Res., 113, D15S17, doi:10.1029/2007JD008819, 2008.

Newell, R. and Gould-Stewart, S.: A Stratospheric Fountain, J. Atmos. Sci., 38, 2789–2796, 1981.

O'Connor, F. M., Carver, G. D., Savag, N. H., Pyle, J. A., Methven, J., Arnold, S. R., Dewey, K., and Kent, J.: Comparison and visualisation of high-resolution transport modelling with aircraft measurements, Atmos. Sci. Lett., 6, 164–170, 2005.

Osterman, G. B., Kulawik, S. S., Worden, H. M., Richards, N. A. D., Fisher, B. M., Eldering, A., Shephard, M. W., Froidevaux, L., Labow, G., Luo, M., Herman, R. L., Bowman, K. W., and Thompson, A. M.: Validation of Tropospheric Emission Spectrometer (TES) measurements of the total, stratospheric, and tropospheric column abundance of ozone, J. Geophys. Res., 113, D15S16, doi:10.1029/2007JD008801, 2008.

Park, M., Randel, W. J., Gettelman, A., Massie, S. T., and Jiang, J. H.: Transport above the Asian summer monsoon anticyclone inferred from Aura Microwave Limb Sounder tracers, J. Geophys. Res., 112, D16309, doi:10.1029/2006JD008294, 2007.

Park, M., Randel, W. J., Emmons, L. K., Bernath, P. F., Walker, K. A., and Boone, C. D.: Chemical isolation in the Asian monsoon anticyclone observed in Atmospheric Chemistry Experiment (ACE-FTS) data, Atmos. Chem. Phys., 8, 757–764, doi:10.5194/acp-8-757-2008, 2008.

Parker, D., Jackson, M., and Horton, E.: The 1961–1990 GISST 2.2 Sea Surface Temperature and Sea Ice Climatology, Climate Research Technical Note No.63, Hadley Centre for Climate Prediction and Research, Bracknell, UK, 1995.

Petch, J. C., Willett, M., Wong, R. Y., and Woolnough, S. J.: Modelling suppressed and active convection. Comparing a numerical weather prediction, cloud-resolving and single-column model, Q. J. Roy. Meteorol. Soc., 133, 1087–1100, doi:10.1002/qj.109, 2007.

Prather, M.: Numerical advection by conservation of 2nd-order moments, J. Geophys. Res., 91, 6671–6681, 1986.

Priestley, A.: A quasi-conservative version of the semi-lagrangian advection scheme, Mon. Weather Rev., 121, 621–629, 1993.

Randel, W. J. and Park, M.: Deep convective influence on the Asian summer monsoon anticyclone and associated tracer variability observed with Atmospheric Infrared Sounder (AIRS), J. Geophys. Res., 111, D12314, doi:10.1029/2005JD006490, 2006.

Randel, W. J., Park, M., Emmons, L., Kinnison, D., Bernath, P., Walker, K. A., Boone, C., and Pumphrey, H.: Asian Monsoon Transport of Pollution to the Stratosphere, Science, 328, 611–613, doi:10.1126/science.1182274, 2010.

Ricaud, P., Barret, B., Attié, J.-L., Motte, E., Le Flochmoën, E., Teyssèdre, H., Peuch, V.-H., Livesey, N., Lambert, A., and Pommereau, J.-P.: Impact of land convection on troposphere-stratosphere exchange in the tropics, Atmos. Chem. Phys., 7, 5639–5657, doi:10.5194/acp-7-5639-2007, 2007.

Richards, N. A. D., Osterman, G. B., Browell, E. V., Hair, J. W., Avery, M., and Li, Q.: Validation of Tropospheric Emission Spectrometer ozone profiles with aircraft observations during the intercontinental chemical transport experiment-B, J. Geophys. Res., 113, D16S29, doi:10.1029/2007JD008815, 2008.

Rind, D., Lerner, J., Jonas, J., and McLinden, C.: Effects of resolution and model physics on tracer transports in the NASA Goddard Institute for Space Studies general circulation models, J. Geophys. Res., 112, D09315, doi:10.1029/2006JD007476, 2007.

Rodgers, C. D. and Connor, B. J.: Intercomparison of remote sounding instruments, J. Geophys. Res., 108(D3), 4116, doi:10.1029/2002JD002299, 2003.

Rossow, W., Walker, A., Beuschel, D., and Roiter, M.: International Satellite Cloud Climatology Project (ISCCP) Documentation of New Cloud Datasets, Tech. Rep. WMO/TD-No. 737, World Meteorological Organization, 1996.

Russo, M. R., Marécal, V., Hoyle, C. R., Arteta, J., Chemel, C., Chipperfield, M. P., Dessens, O., Feng, W., Hosking, J. S., Telford, P. J., Wild, O., Yang, X., and Pyle, J. A.: Representation of tropical deep convection in atmospheric models – Part 1: Meteorology and comparison with satellite observations, Atmos. Chem. Phys., 11, 2765–2786, doi:10.5194/acp-11-2765-2011, 2011.

Salawitch, R. J., Weisenstein, D. K., Kovalenko, L. J., Sioris, C. E., Wennberg, P. O., Chance, K., Ko, M. K. W., and McLinden, C. A.: Sensitivity of ozone to bromine in the lower stratosphere, Geophys. Res. Lett., 32, L05811, doi:10.1029/2004GL021504, 2005.

Sander, S. P., Friedl, R. R., Ravishankara, A. R., Golden,D. M., Kolb, C. E., Kurylo, M. J., Huie, R. E., Orkin V. L., Molina, M. J., Moortgat, G. K., and Finlayson-Pitts, B. J.: Chemical Kinetics and Photochemical Data for Use in Atmospheric Studies, Tech. rep., JPL, 2003.

Sherwood, S. C. and Dessler, A. E.: On the control of stratospheric humidity, Geophys. Res. Lett., 27, 2513–2516, 2000.

Shindell, D. T., Faluvegi, G., Stevenson, D. S., Krol, M. C., Emmons, L. K., Lamarque, J. F., Petron, G., Dentener, F. J., Ellingsen, K., Schultz, M. G., Wild, O., Amann, M., Atherton, C. S., Bergmann, D. J., Bey, I., Butler, T., Cofala, J., Collins, W. J., Derwent, R. G., Doherty, R. M., Drevet, J., Eskes, H. J., Fiore, A. M., Gauss, M., Hauglustaine, D. A., Horowitz, L. W., Isaksen, I. S. A., Lawrence, M. G., Montanaro, V., Mueller, J. F., Pitari, G., Prather, M. J., Pyle, J. A., Rast, S., Rodriguez, J. M., Sanderson, M. G., Savage, N. H., Strahan, S. E., Sudo, K., Szopa, S., Unger, N., van Noije, T. P. C., and Zeng, G.: Multimodel simulations of carbon monoxide: Comparison with observations and projected near-future changes, J. Geophys. Res., 111, D19306, doi:10.1029/2006JD007100, 2006.

Sinnhuber, B.-M. and Folkins, I.: Estimating the contribution of bromoform to stratospheric bromine and its relation to dehydration in the tropical tropopause layer, Atmos. Chem. Phys., 6, 4755–4761, doi:10.5194/acp-6-4755-2006, 2006.

Skamarock, W. C., Klemp, J. B., Dudhia, J., Gill, D. O., Barker, D. M., Duda, M. G., Huang, X.-Y., Wang, W., and Powers, J. G.: A description of the Advanced Research WRF Version 3, NCAR Technical Note NCAR/TN-475+STR, NCAR, NCAR Boulder, CO, USA, 2008.

Stockwell, D. Z. and Chipperfield, M. P.: A tropospheric chemical-transport model: Development and validation of the model transport schemes, Q. J. Roy. Meteorol. Soc., 125, 1747–1783, 1999.

Sturges, W. T., Oram, D. E., Carpenter, L. J., Penkett, S. A., and Engel, A.: Bromoform as a source of stratospheric bromine, Geophys. Res. Lett., 27, 2081–2084, 2000.

Sukoriansky, S., Galperin, B., and Staroselsky, I.: A quasinormal scale elimination model of turbulent flows with stable stratification, Phys. Fluids, 17, 085107, doi:10.1063/1.2009010, 2005.

Telford, P. J., Braesicke, P., Morgenstern, O., and Pyle, J. A.: Technical Note: Description and assessment of a nudged version of the new dynamics Unified Model, Atmos. Chem. Phys., 8, 1701–1712, doi:10.5194/acp-8-1701-2008, 2008.

Tian, W. and Chipperfield, M.: A new coupled chemistry-climate model for the stratosphere: The importance of coupling for future O-3-climate predictions, Q. J. Roy. Meteorol. Soc., 131, 281–303, doi:10.1256/qj.04.05, 2005.

Tiedtke, M.: A comprehensive mass flux scheme for cumulus parameterization in large-scale models, Mon. Weather Rev., 117, 1779–1800, 1989.

Tost, H., Lawrence, M. G., Brühl, C., and Jöckel, P.: The GABRIEL Team, and The SCOUT-O3-DARWIN/ACTIVE Team: Uncertainties in atmospheric chemistry modelling due to convection parameterisations and subsequent scavenging, Atmos. Chem. Phys., 10, 1931–1951, doi:10.5194/acp-10-1931-2010, 2010.

Tremback, C. J., Powell, J., Cotton, W. R., and Pielke, R. A.: the forward-in-time upstream advection scheme – extension to higher orders, Mon. Weather Rev., 115, 540–555, 1987.

Vaughan, G., Schiller, C., MacKenzie, A. R., Bower, K., Peter, T., Schlager, H., Harris, N. R. P., and May, P. T.: Studies in a natu-

ral laboratory: High-altitude aircraft measurements around deep tropical convection, B. Am. Meteorol. Soc., 89, 647–662, 2008.

Viciani, S., D'Amato, F., Mazzinghi, P., Castagnoli, F., Toci, G., and Werle, P.: A cryogenically operated laser diode spectrometer for airborne measurement of stratospheric trace gases, Appl. Phy. B, 90, 581–592, doi:10.1007/s00340-007-2885-2, 2008.

Wang, J. S., McElroy, M. B., Logan, J. A., Palmer, P. I., Chameides, W. L., Wang, Y., and Megretskaia, I. A.: A quantitative assessment of uncertainties affecting estimates of global mean OH derived from methyl chloroform observations, J. Geophys. Res., 113, D12302, doi:10.1029/2007JD008496, 2008.

Wang, K., Pyle, J., Sanderson, M., and Bridgeman, C.: Implementation of a convective atmospheric boundary layer scheme in a tropospheric chemistry transport model, J. Geophys. Res., 104, 23729–23745, 1999.

Wicker, L. and Skamarock, W.: Time-splitting methods for elastic models using forward time schemes, Mon. Weather Rev., 130, 2088–2097, 2002.

Wild, O. and Prather, M. J.: Global tropospheric ozone modeling: Quantifying errors due to grid resolution, J. Geophys. Res., 111, D11305, doi:10.1029/2005JD006605, 2006.

Wild, O., Prather, M., Akimoto, H., Sundet, J., Isaksen, I., Crawford, J., Davis, D., Avery, M., Kondo, Y., Sachse, G., and Sandholm, S.: Chemical transport model ozone simulations for spring 2001 over the western Pacific: Regional ozone production and its global impacts, J. Geophys. Res., 109, D15S02, doi:10.1029/2003JD004041, 2004.

Willmott, C., Rowe, C., and Mintz, Y.: Climatology of the terrestrial seasonal water cycle, J. Climatol., 5, 589–606, 1985.

Worden, H. M., Logan, J. A., Worden, J. R., Beer, R., Bowman, K., Clough, S. A., Eldering, A., Fisher, B. M., Gunson, M. R., Herman, R. L., Kulawik, S. S., Lampel, M. C., Luo, M., Megretskaia, I. A., Osterman, G. B., and Shephard, M. W.: Comparisons of Tropospheric Emission Spectrometer (TES) ozone profiles to ozonesondes: Methods and initial results, J. Geophys. Res., 112, D03309, doi:10.1029/2006JD007258, 2007.

Zalesak, S.: Fully multidimensional flux-corrected transport algorithms for fluids, J. Comput. Phys., 31, 335–362, 1979.

Zeng, G. and Pyle, J.: Changes in tropospheric ozone between 2000 and 2100 modeled in a chemistry-climate model, Geophys. Res. Lett., 30, 1392, doi:10.1029/2002GL016708, 2003.